MNRAS **456,** 617–632 (2016) doi:10.1093/mnras/stv2636

The AIMSS Project – III. The stellar populations of compact stellar systems

Joachim Janz,[1⋆] Mark A. Norris,[2,3] Duncan A. Forbes,[1] Avon Huxor,[4] Aaron J. Romanowsky,[5,6] Matthias J. Frank,[7] Carlos G. Escudero,[8,9,10] Favio R. Faifer,[8,9,10] Juan Carlos Forte,[10,11] Sheila J. Kannappan,[12] Claudia Maraston,[13] Jean P. Brodie,[6] Jay Strader[14] and Bradley R. Thompson[5]

[1] *Centre for Astrophysics & Supercomputing, Swinburne University, Hawthorn, VIC 3122, Australia*
[2] *Max Planck Institut für Astronomie, Königstuhl 17, D-69117 Heidelberg, Germany*
[3] *Jeremiah Horrocks Institute, University of Central Lancashire, Preston PR1 2HE, UK*
[4] *Astronomisches Rechen-Institut, Zentrum für Astronomie der Universität Heidelberg, Mönchstraße 12-14, D-69120 Heidelberg, Germany*
[5] *Department of Physics and Astronomy, San José State University, One Washington Square, San Jose, CA 95192, USA*
[6] *University of California Observatories, 1156 High Street, Santa Cruz, CA 95064, USA*
[7] *Landessternwarte, Zentrum für Astronomie der Universität Heidelberg, Königsstuhl 12, D-69117 Heidelberg, Germany*
[8] *Facultad de Cs. Astronómicas y Geofísicas, UNLP, Paseo del Bosque S/N, 1900 La Plata, Argentina*
[9] *Instituto de Astrofísica de La Plata (CCT La Plata - CONICET - UNLP), Paseo del Bosque S/N, B1900FWA La Plata, Argentina*
[10] *Consejo Nacional de Investigaciones Científicas y Técnicas, Rivadavia 1917, C1033AAJ Ciudad Autónoma de Buenos Aires, Argentina*
[11] *Planetario 'Galileo Galilei', Secretaría de Cultura, CP1425 Ciudad Autónoma de Buenos Aires, Argentina*
[12] *Department of Physics and Astronomy, UNC-Chapel Hill, CB3255, Phillips Hall, Chapel Hill, NC 27599, USA*
[13] *Institute of Cosmology and Gravitation, Dennis Sciama Building, Burnaby Road, Portsmouth PO1 3FX, UK*
[14] *Department of Physics and Astronomy, Michigan State University, East Lansing, MI 48824, USA*

Accepted 2015 November 6. Received 2015 November 5; in original form 2015 September 30

ABSTRACT

In recent years, a growing zoo of compact stellar systems (CSSs) have been found whose physical properties (mass, size, velocity dispersion) place them between classical globular clusters (GCs) and true galaxies, leading to debates about their nature. Here we present results using a so far underutilized discriminant, their stellar population properties. Based on new spectroscopy from 8–10m telescopes, we derive ages, metallicities, and [α/Fe] of 29 CSSs. These range from GCs with sizes of merely a few parsec to compact ellipticals (cEs) larger than M32. Together with a literature compilation, this provides a panoramic view of the stellar population characteristics of early-type systems. We find that the CSSs are predominantly more metal rich than typical galaxies at the same stellar mass. At high mass, the cEs depart from the mass–metallicity relation of massive early-type galaxies, which forms a continuous sequence with dwarf galaxies. At lower mass, the metallicity distribution of ultracompact dwarfs (UCDs) changes at a few times 10^7 $M_\odot$, which roughly coincides with the mass where luminosity function arguments previously suggested the GC population ends. The highest metallicities in CSSs are paralleled only by those of dwarf galaxy nuclei and the central parts of massive early types. These findings can be interpreted as CSSs previously being more massive and undergoing tidal interactions to obtain their current mass and compact size. Such an interpretation is supported by CSSs with direct evidence for tidal stripping, and by an examination of the CSS internal escape velocities.

Key words: galaxies: fundamental parameters – galaxies: stellar content.

1 INTRODUCTION

At the dawn of the millennium, the distinction between star clusters and galaxies was apparently clear. The parameter space, e.g. in radius versus mass, between globular clusters (GCs) and galaxies was

⋆E-mail: jjanz@swin.edu.au

essentially empty, allowing simple selections in observed properties to be made in order to separate star clusters and galaxies. The field came to life with the discovery of a population of compact stellar systems (CSSs) that started to fill in the parameter space between star clusters and bona-fide galaxies. The objects initially appeared in two main groups. On the lower mass end ($M_* \gtrsim 10^6$–10^8 M$_\odot$) ultra-compact dwarfs (UCDs; Hilker et al. 1999; Drinkwater et al. 2000) emerged from the classical GC population, while on the higher mass end ($\gtrsim 10^9$ M$_\odot$) the hitherto apparently rare compact ellipticals (cEs) were found to be relatively common (e.g. Mieske et al. 2005; Chilingarian et al. 2007, 2009; Smith Castelli et al. 2008; Price et al. 2009; Norris et al. 2014; Chilingarian & Zolotukhin 2015). More recently the gap between star clusters and galaxies has finally been completely filled by systematic searches for CSSs, such as the first study in this series [*A*rchive of *I*ntermediate *M*ass *S*tellar *S*ystems (AIMSS) Survey; Norris et al. 2014, hereafter AIMSS I].

The final closing of the gap between star clusters and massive galaxies called into question the exact separation to be used to divide them, and even whether there was a fundamental difference between them at all (e.g. Forbes & Kroupa 2011; Forbes et al. 2011; Willman & Strader 2012). In parallel to this debate, the emergence of an apparently tight scaling relation of size as function of stellar mass gave rise to the enticing prospect that it might be possible to unify all dynamically hot stellar systems from GCs to galaxies (e.g. Kissler-Patig, Jordán & Bastian 2006; Misgeld et al. 2011) within a single formation scenario. However, the subsequent discovery of additional objects which broadened the distributions of CSSs challenged this idea (see e.g. Brodie et al. 2011; Forbes et al. 2013). Despite the confusion caused by the burst of newly discovered CSS types, one recurring theme for CSSs over the whole mass range from UCDs to cEs is the suggestion that stripping processes play a role in their formation (e.g. Bassino, Muzzio & Rabolli 1994; Bekki, Couch & Drinkwater 2001; Choi, Guhathakurta & Johnston 2002; Drinkwater et al. 2003; Bekki & Couch 2003).

Today, there is little doubt that the tidal stripping of galaxies leads to the formation of many CSSs. The evidence for this is compelling and varied, from CSSs caught in the act of formation and still embedded in tidal streams of stars from their disrupted progenitors (Huxor, Phillipps & Price 2013; Foster et al. 2014; Jennings et al. 2015), to individual CSSs which host central supermassive black holes with masses expected to be found only in much more massive galaxies (Kormendy et al. 1997; Seth et al. 2014). Furthermore, CSSs display stellar populations more akin to those of significantly more massive galaxies than to those of galaxies of similar mass (e.g. Chilingarian et al. 2009; Francis et al. 2012; Sandoval et al. 2015). Finally there is the example of NGC 4546-UCD1 which is found to have a star formation history (SFH) which extends over several Gyr, a feat unlikely for a star cluster (Norris et al. 2015).

Complicating this picture is the fact that there is also growing evidence that on either end of the CSS mass distribution many objects are simply continuations of the adjacent populations. Extrapolation of the GC luminosity functions of galaxies indicates that many if not most UCDs are simply GCs more massive than those found around the Milky Way, and which are only found in galaxies with sufficiently rich GC populations (e.g. Fellhauer & Kroupa 2002, 2005; Hilker 2006; Norris & Kannappan 2011; Mieske, Hilker & Misgeld 2012). Likewise there are suggestions that some cE galaxies may comprise the low-mass tail of the true elliptical galaxy population (see e.g. Kormendy et al. 2009), rather than the end result of the tidal stripping of larger galaxies. Counterintuitively, a further indication that the mechanisms responsible for forming CSSs may in fact be varied comes from the observation that they are found to be relatively ubiquitous. Both UCDs and cEs can be located in all galactic environments from field (where tidal stripping is unlikely to be responsible) to dense galaxy clusters (AIMSS I; Norris & Kannappan 2011; Huxor et al. 2013; Paudel et al. 2014; Chilingarian & Zolotukhin 2015). As some CSSs are known to form by stripping, and still others are found in environments where stripping is currently impossible, it seems to suggest that at least one other formation mechanism is at work (or those are run-aways that were stripped in a cluster and have been ejected via three body interaction, see Chilingarian & Zolotukhin 2015).

Given the on-going discussion, new discoveries, and recent success in obtaining sizeable samples, the time is now ripe to reexamine the information provided by the stellar populations of CSSs. What can the stellar populations of CSSs reveal about their formation history, and can they be used as a discriminant between stripped objects and those that formed via other mechanisms?

In this paper, we report on the analysis of the integrated stellar populations. The sample is introduced in the following Section 2, and the observations are described in Section 3. Section 4 details the procedure followed to obtain ages, metallicities, and [α/Fe] for all objects, while the results thereof are presented in Section 5. The results are further discussed in Section 6 and we conclude with a summary of our findings in the final Section 7.

2 SAMPLE

Our aim is to construct the largest possible sample of CSSs and comparison objects [elliptical, lenticular (dEs), dwarf spheroidals (dSphs), and early-type dwarf galaxies (E/S0s)] with accurate spectroscopically derived stellar population parameters. We therefore combine a large catalogue of literature data for CSSs and associated objects with new spectroscopic observations obtained with the Large Binocular Telescope (LBT), Keck II and Gemini South telescopes, targeted to fill in regions of parameter space which were previously undersampled.

We draw our sample for new spectroscopic observation principally from two main sources. The first is from Paper I of the AIMSS project (AIMSS I), and the second is a new catalogue of cE galaxies selected from the SDSS (Huxor et al., in preparation). To increase the sample size further, and to broaden the range of parameter space studied, we have also observed additional literature CSSs which previously lacked suitable spectroscopically derived stellar population parameters. Furthermore, we include M60-UCD2 and VCC 165cE. These two objects were identified through using SDSS to select for UCD candidates based on colour, magnitude, and apparent size (see Sandoval et al. 2015). M60-UCD2 was subsequently reported as a UCD candidate in the Next Generation Virgo Cluster Survey (NGVS-J124352.42+112534.2; Liu et al. 2015b), and we adopt their photometric parameters for this object.

Note that our LBT/MODS spectroscopic observations were generally carried out as filler and bad weather programmes, and therefore tends to preferentially focus on brighter, easier to observe targets. An overview of our full sample together with the comparison objects is shown in the mass–stellar size plane in Fig. 1.

When selecting the literature comparison sample, we aimed at broadly sampling the population of dynamically hot stellar systems from the most massive early-type galaxies to CSSs from GCs to cEs. We required that the objects had spectroscopically determined stellar populations measurements and, in regions of parameter space for which there are many studies, we restricted the selection to

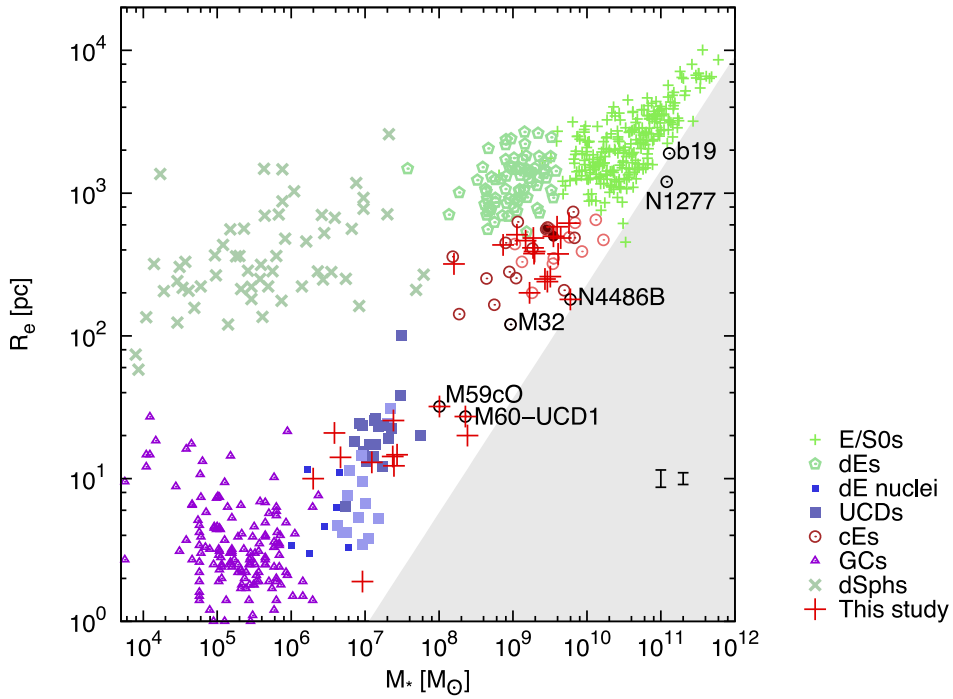

Figure 1. Size versus stellar mass plot for our sample objects, as well as other CSSs from the literature, and several comparison samples of various types of objects. CSSs without a measurement of [α/Fe] are plotted with lighter colour. Two isolated cEs (Huxor et al. 2013; Paudel et al. 2014) are highlighted with filled dark red symbols. Several objects that deserve special attention are named in the plot (see text for details; b19 is short for SDSS J151741.75−004217.6). Typical uncertainties for the sizes are shown in the lower-right corner: the smaller bar for most of the CSSs and the larger for those within extended light, e.g. within streams, and dSphs. The grey shaded area indicates the zone of avoidance, which Misgeld & Hilker (2011) found to be devoid of stellar systems.

homogenous sources with large samples. Our sources for the literature data are:

(i) GCs – the Harris Milky Way GC catalogue (Harris 1996, 2010 edition), with ages for 55 MW GCs from VandenBerg et al. (2013), and [α/Fe] for 43 GCs from the compilation in Pritzl, Venn & Irwin (2005).

(ii) UCDs – Paudel, Lisker & Janz (2010b), Chiboucas et al. (2011), Chilingarian et al. (2011), and Francis et al. (2012), with the photometry for some of the objects taken from Haşegan et al. (2005), Evstigneeva et al. (2007), Mieske & Kroupa (2008), and Zhang et al. (2015).

(iii) cEs – Chilingarian et al. (2007), Chilingarian et al. (2009), Price et al. (2009), Huxor et al. (2011b), Huxor et al. (2013), Paudel et al. (2014), and Guérou et al. (2015).

(iv) dSphs – structural parameters and metallicities for Local Group dwarf spheroidal data are from McConnachie (2012). Unfortunately, no luminosity weighted age or [α/Fe] information exists for these objects due to their low surface brightness. We include mass weighted ages for some objects from Orban et al. (2008) as upper limits for the luminosity weighted ages.

(v) dEs – Chilingarian (2009), Paudel, Lisker & Kuntschner (2011, main body of the dE after subtraction of nucleus), and Toloba et al. (2014) with photometry and sizes from Janz & Lisker (2008, 2009)

(vi) dE nuclei – Paudel et al. (2011) with sizes from Côté et al. (2006)

(vii) E/S0s – the ATLAS^{3D} survey (Cappellari et al. 2011) with stellar population parameters from McDermid et al. (2015), and using the multi-Gaussian expansions of Scott et al. (2013) to estimate the stellar mass within $R_e/8$.

Where possible we convert iron abundances to total metallicities using $[Z/H] = [Fe/H] + 0.94[\alpha/Fe]$ (Thomas, Maraston & Bender 2003), and where this is not possible we indicate objects without [α/Fe] measurements, as for these objects the metallicity value is an approximation and is too low if the object is α-enhanced.

3 OBSERVATIONS AND DATA REDUCTION

In total to date we have obtained spectroscopy of 29 objects at the LBT, Keck and Gemini observatories. Table 1 provides the full observing log of the targets observed in this work, and in Fig. 2 a sample spectrum for each telescope is shown.

3.1 LBT MODS

Observations of 19 of our CSSs were obtained with the first multi-object double spectrograph (MODS1; Pogge et al. 2010) on the LBT. MODS1 provides simultaneously observation of both a blue and red arm, providing spectral coverage from ∼3200 to 10 000 Å split at around 5700 Å. For this study, we primarily focus on the blue arm which covers all of the main Lick absorption line indices and provides a spectral resolution of ∼2.3 Å FWHM (full width at half-maximum), for our chosen slit width of 0.8 arcsec measured at around 5000 Å. Typical exposure times are of the order of 3600 s per target.

The MODS spectroscopy was reduced using the beta-release of the MODS reduction pipeline.[1] This reduction comprised bias

[1] The MODS reduction pipeline was developed by K. Croxall with funding from NSF Grant AST-1108693. Details can be found at http://www.astronomy.ohio-state.edu/MODS/Software/modsIDL/.

Table 1. Observing log.

Name	RA (J2000)	Dec. (J2000)	Date (dd-mm-yy)	Telescope /Instrument	Setup
2MASX J01491447+1301548	01:49:14.45	+13:01:55.1	28-10-14	Keck/ESI	0.75 arcsec 2400 s 1.1 Å 0.8 arcsec
NGC 1128cE	02:57:44.50	+06:02:02.2	28-10-14	Keck/ESI	0.75 arcsec 1800 s 1.1 Å 0.9 arcsec
			05-10-13–15-02-14	LBT/MODS	0.8 arcsec 9246 s 2.3 Å 1.3 arcsec
NGC 1272cE	03:19:23.04	+41:29:28.2	28-10-14	Keck/ESI	0.75 arcsec 2400 s 1.1 Å 0.8 arcsec
SDSS J075140.40+501102.6	07:51:40.39	+50:11:02.6	15-02-14	LBT/MODS	0.8 arcsec 7200 s 2.3 Å 1.5 arcsec
			28-10-14	Keck/ESI	0.75 arcsec 1200 s 1.1 Å 0.6 arcsec
NGC 2832cE	09:19:47.90	+33:46:04.9	21-02-14	LBT/MODS	0.8 arcsec 1800 s 2.3 Å 1.2 arcsec
			21-02-14	Keck/ESI	0.75 arcsec 3600 s 1.1 Å 0.7 arcsec
NGC 2892cE	09:32:53.90	+67:36:54.5	16-02-14	LBT/MODS	0.8 arcsec 5400 s 2.3 Å 1.0 arcsec
cE0	09:47:29.23	+14:12:45.3	16-02-14	LBT/MODS	0.8 arcsec 2700 s 2.3 Å 1.0 arcsec
CGCG 036-042	10:08:10.32	+02:27:48.3	21-02-14	LBT/MODS	0.8 arcsec 1800 s 2.3 Å 1.2 arcsec
cE1	11:04:04.40	+45:16:18.9	16–17-02-14	LBT/MODS	0.8 arcsec 5400 s 2.3 Å 1.0 arcsec
NGC 3628-UCD1	11:21:01.20	+13:36:29.3	21-03-14	Keck/ESI	0.75 arcsec 3600 s 1.1 Å 0.7 arcsec
			13–14-06-15	LBT/MODS	0.80 arcsec 3600 s 2.3 Å 1.2 arcsec
NGC 3923-UCD1	11:51:04.10	−28:48:19.8	30-04-11	Gemini/GMOS	0.5 arcsec 10 800 s 1.26 Å 0.9 arcsec
NGC 3923-UCD2	11:50:55.90	−28:48:18.4	30-04-11	Gemini/GMOS	0.5 arcsec 10 800 s 1.26 Å 0.9 arcsec
NGC 3923-UCD3	11:51:05.20	−28:48:58.9	30-04-11	Gemini/GMOS	0.5 arcsec 10 800 s 1.26 Å 0.9 arcsec
PGC 038205	12:04:28.97	+01:53:38.8	20-02-14	LBT/MODS	0.8 arcsec 2400 s 2.3 Å 1.2 arcsec
M85-HCC1	12:25:22.84	+18:10:53.6	04–06-04-14	LBT/MODS	0.8 arcsec 5400 s 2.3 Å 1.4 arcsec
NGC 4486B/VCC1297	12:30:31.97	+12:29:24.6	10-03-15	LBT/MODS	0.8 arcsec 1800 s 2.3 Å 0.9 arcsec
S999	12:30:45.91	+12:25:01.5	21-03-14	Keck/ESI	0.75 arcsec 11 400 s 1.1 Å 0.6 arcsec
NGC 4546-UCD1	12:35:28.70	−03:47:21.1	02-07-13–07-01-14	Gemini/GMOS	0.5 arcsec 22 200 s 1.41 Å 0.7 arcsec
Sombrero-UCD1	12:40:03.13	−11:40:04.3	15-03-15	LBT/MODS	0.8 arcsec 2700 s 2.3 Å 1.5 arcsec
M59cO	12:41:55.33	+11:40:03.7	10-03-15	LBT/MODS	0.8 arcsec 3600 s 2.3 Å 1.1 arcsec
M59-UCD3	12:42:11.05	+11:38:41.2	17-02-14	LBT/MODS	0.8 arcsec 3000 s 2.3 Å 1.1 arcsec
			21-03-14	Keck/ESI	0.75 arcsec 1200 s 1.1 Å 0.7 arcsec
M60-UCD1	12:43:36.00	+11:32:04.6	06-04-14 and 10-03-15	LBT/MODS	0.8 arcsec 6300 s 2.3 Å 1.5 and 0.8 arcsec
M60-UCD2	12:43:52.41	+11:25:34.2	15-03-15	LBT/MODS	0.8 arcsec 3600 s 2.3 Å 1.8 arcsec
SDSS J133842.45+311457.0	13:38:42.45	+31:14:57.1	30-03-14	LBT/MODS	0.8 arcsec 2700 s 2.3 Å 2.0 arcsec
NGC 5846cE	15:06:34.27	+01:33:31.6	12-03-15	LBT/MODS	0.8 arcsec 1800 s 2.3 Å 1.5 arcsec
2MASX J16053723+1424418	16:05:37.21	+14:24:41.3	21-03-14	Keck/ESI	0.75 arcsec 1800 s 1.1 Å 0.7 arcsec
cE2	23:15:12.62	−01:14:58.3	14-06-15	LBT/MODS	0.8 arcsec 2700 s 2.3 Å 1 arcsec
J233829.31+270225.1	23:38:29.31	+27:02:25.1	28-10-14	Keck/ESI	0.75 arcsec 2400 s 1.1 Å 0.7 arcsec

Notes. The setup lists the slitwidth, exposure time, spectral resolution (FWHM, measured at around 5000 Å) and seeing. M60-UCD1 is also known as NGC 4649-UCD1, and NGC 1128cE as NGC 1128-AIMSS2.

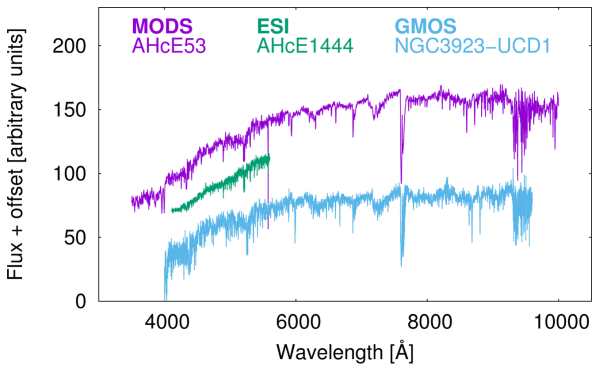

Figure 2. Example spectra observed with MODS, GMOS, and ESI, showing the different wavelength coverage. Arbitrary scaling and offsets are applied to the fluxes for clarity. For MODS and ESI, the very bluest ∼200 Å are omitted, as they are of very low S/N and are not used in the analysis. At the red end the ESI spectrum is restricted to the wavelength range of the comparison spectrum for joining the echelle orders (see text for details).

subtraction and flat-fielding using PYTHON scripts which deal with the effects of MODS interlaced data readout, followed by wavelength calibration, object tracing and extraction, and finally flux calibration using observations of flux standard stars observed during each observing run. We confirmed the reliability of the flux calibration procedure by comparing the overlap region of the spectra produced by the reduction pipeline for the blue and red spectrographs.

3.2 Gemini GMOS

We incorporate very high quality spectra of four objects obtained with Gemini Multi-Object Spectrograph (GMOS; Hook et al. 2004) at Gemini-South. The data for three NGC 3923 UCDs were reduced and first presented in Norris et al. (2012), with the velocity dispersions measured in the AIMSS I paper. The observations were carried out in the multi-object mode with the 1200 l/mm grating and 0.5 arcsec slitlets, resulting in a spectral resolution of 1.26 Å, again measured around 5000 Å. For each of the three objects, there were six individual spectra with exposure times of 1800 s each. The spectrum for NGC 4546-UCD1 (Norris et al. 2015 and Escudero et al., in preparation) was observed with essentially the same setup (with a spectral resolution of 1.41 Å) and reduced using the same procedure. The total integration time was 22 200 s split over 12 individual exposures. In our chosen setup GMOS spectra cover a wavelength range from ∼4100 to 5600 Å, which means that one to three of the bluest Lick indices in the stellar population analysis are missed (depending on the exact location of the slitlet on the mask).

3.3 Keck ESI

The spectra of nine objects were taken with the echellette spectrograph and imager (ESI; Sheinis et al. 2002) on the Keck II telescope. The observations of each object were split into at least three individual exposures. The total integration times ranged from 1200 to 11400 s. The instrument was used in the echellette mode with a slit width of 0.75 arcsec. The wavelength range covered exceeds 4000 to 10 000 Å across 10 echelle orders, but the bluest and reddest parts are swamped in noise. For the stellar population analysis, we concentrated on a region from 4050 to 5500 Å (in the rest frame) with the Lick indices used for the model fitting.

The standard steps for the data reduction are conducted with MAKEE.[2] The echelle characteristic of the spectrograph requires an additional step to bring the flux measurements in the different orders to a common level, and to join them for a uniform coverage of the whole spectral range. For that purpose we compared the spectrum of a star observed under the same conditions to its reference spectrum (Le Borgne et al. 2003). The individual exposures and orders were combined in an S/N optimized way with UVES_POPLER.[3] The individual errors of the spectral pixels were also propagated to produce a combined error spectrum. The instrumental resolution of this setup is ∼1.1 Å (FWHM, measured around 5000 Å) and thus higher than with MODS. The spectra were re-dispersed to 1 Å pix^{-1} for the further analysis.

We include the UCDs S999 (Janz et al. 2015) and NGC 3628-UCD1 (Jennings et al. 2015) in the sample, for which the same procedures were followed. Five objects were observed twice with different instruments. We used these spectra to ensure that the stellar population analysis yields consistent results across the different observations (see appendix). Likewise, we additionally analysed SDSS spectra of four objects for further comparison, and include results based on the SDSS spectrum of VCC 165cE (see Section 5.1.4). For the subsequent analysis we use the error weighted averages of the stellar population parameters for the objects with multiple sets.

3.4 Photometry

Our sample of CSSs is based on the catalogue of AIMSS I plus additional cEs selected from the SDSS by Huxor et al. (in preparation). The photometry and size measurements were adopted from these studies and we refer the reader to them for a detailed description of the analysis. In summary, AIMSS I made use of *HST* WFPC2, ACS or WFC3 imaging to provide accurate size estimates and supplemented the available *HST* imaging (which was generally only single or two band) with photometry from a variety of ground-based sources to provide wider wavelength coverage. Huxor et al. (in preparation) use catalogued SDSS photometry except where the target is judged to be deeply embedded in the halo of a larger galaxy. In this case the host galaxy light was subtracted following a scheme similar to that outlined in AIMSS I. Total magnitudes were then obtained with a curve-of-growth method and corrected for Galactic extinction following Schlafly & Finkbeiner (2011).

For conversion to absolute magnitudes and physical scales, we used the distance of the host galaxy, where applicable, or estimated the distance based on the object's recession velocity assuming a Hubble flow with $H_0 = 68$ km s^{-1} Mpc^{-1}. The absolute magnitudes were converted to stellar mass using the mass-to-light ratios from Maraston (2005) and the stellar populations measured here, assuming a Kroupa initial stellar mass function. Note that for high-mass UCDs the initial mass function (IMF) is debated (Dabringhausen, Hilker & Kroupa 2008; Mieske et al. 2008), but the potential resulting shift in stellar mass does not change any of our conclusions (∼0.27 dex in log M_* when changing from Kroupa to Salpeter IMF, with nearly no difference for the model Lick indices; see Maraston et al. 2003). If the photometry was available in multiple filters, we used the reddest band when calculating the stellar mass. A comparison to the previously used AIMSS stellar masses can be found in the appendix. For the literature samples, we used the literature stellar masses when quoted, and followed the same procedure otherwise.

4 ANALYSIS

All the reduced spectra were used as input to measure Lick line indices using the definitions of Trager et al. (1998) with LECTOR.[4] The measurements include 19 indices from Hδ_A to Fe5406. With PPXF (Cappellari & Emsellem 2004) the line-of-sight velocity distribution was fitted as well as a tenth order multiplicative polynomial to adjust the shape of the continuum. As templates we used the ELODIE library of stellar spectra (Prugniel et al. 2007). The polynomial was used to test whether the analysis for spectra that were not properly flux calibrated (especially the ESI spectra) could be biased. The effect on the final stellar population parameters was found to be negligible. A Monte Carlo run with 50 random realizations of each spectrum using the error spectrum was carried out to obtain the statistical uncertainties of the index measurements.

The measured Lick indices need to be compared to model predictions in order to obtain stellar population characteristics such as age, metallicity, and [α/Fe]. For that the Lick indices need to be measured at the same resolution as the models and corrected for offsets caused by the line-of-sight velocity distributions. We used the best-fitting template and the corresponding spectrum broadened to the object's velocity dispersion to obtain the offsets. The corrections for the higher moments in the velocity distributions are small and thus neglected. Then we interpolated the Lick index predictions of the high-resolution (2.5 Å FWHM) single stellar population (SSP) models of Thomas, Maraston & Johansson (2011) to a fine grid in log age, [Z/H], and [α/Fe] (0.02 dex in each direction) and used χ^2 minimization to find the best-fitting model. For this process two different sets of indices were used: a simple set of indices similar to ATLAS^{3D} (H β, Mgb, Fe5270, and Fe5335) and the full set of indices. For the latter case an iterative σ clipping was applied to remove outliers, but the final set of indices was required to contain at least six indices including one Balmer line, and a magnesium or iron index. A comparison of the resulting stellar population parameters is given in the appendix, as well as a comparison with literature stellar population parameters, and shows generally very good agreement. The so obtained quantities are luminosity weighted.

Generally, the small angular scale of the objects and the seeing during the observations mean that the spectra are integrated over large apertures, and the resulting stellar population parameters are (luminosity-weighted) averages representative for the objects as a whole.

[2] Written by T. Barlow, http://www2.keck.hawaii.edu/inst/esi/makee.html.
[3] Written by M. T. Murphy, http://astronomy.swin.edu.au/∼mmurphy/UVES_popler/.
[4] Written by A. Vazdekis, http://www.iac.es/galeria/vazdekis/vazdekis_software.html.

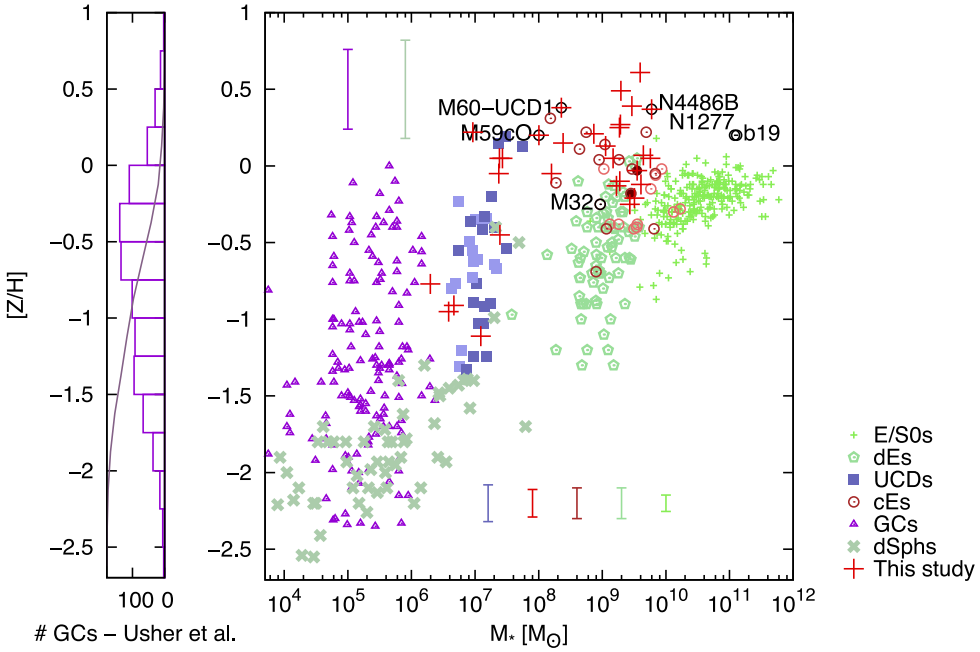

Figure 3. Metallicity versus stellar mass for the same objects as in Fig. 1. Typical error bars are given in the top and bottom parts of the main panel in the respective colours (for the GCs those of Usher et al. 2012 are shown). Additionally, in the left-hand panel the combined metallicity distribution of extragalactic GCs around various early-type galaxies from Usher et al. (2012) is shown as a histogram, as well as the cumulative distribution. The two isolated cEs of Huxor et al. (2013) and Paudel et al. (2014) are highlighted with filled dark red symbols. CSSs with lighter symbol colour are from the literature, but without any measurement of [α/Fe] (so their total metallicity is less secure). The extremely high metallicity of most CSSs becomes evident, not only when compared to objects at the same stellar mass, but also generally.

5 RESULTS

The metallicities from our stellar population analysis are shown in Fig. 3. The comparison samples trace from dwarf spheroidals to giant ellipticals the well-known mass–metallicity relation (see e.g. Gallazzi et al. 2006; Thomas et al. 2010, for large samples of massive early types from SDSS) over many orders of magnitude in stellar mass, with only the most massive galaxies reaching solar metallicities. Our CSSs are almost exclusively more metal rich than the comparison galaxies. Especially when compared at constant stellar mass, they are clearly different. While this applies also to the literature cEs, some of our CSSs are the most metal-rich objects. Most of the literature UCDs are less metal rich than our most extreme low-mass CSSs. Metallicities similar to those in the CSSs are basically only found in the inner regions of galaxies (Fig. 4), such as the inner parts of the ATLAS^{3D} galaxies (McDermid et al. 2015). At lower masses, the nuclei of dEs can have exceedingly high metallicities, when compared to the overall mass–metallicity relation.

The metallicities, as well as stellar ages and [α/Fe], are shown as parameters in the size stellar mass plane in Fig. 5, with all parameters also being listed in Table 2. For the metallicities it can be seen again that the CSSs are more metal rich than more diffuse galaxies at the same mass. Another aspect becomes evident. Overall the metallicities seem to increase along lines of increasing velocity dispersion, rather than stellar mass, as observed also for more massive galaxies (e.g. Guérou et al. 2015; McDermid et al. 2015, compare also to the surface densities in Fig. 6). Turning to stellar ages, compact objects at the low- and high-mass end, i.e. GCs and giant early-type galaxies, are generally old. While this applies also to quite a number of CSSs, many of those studied here exhibit ages of ∼2–8 Gyr. Finally, the CSSs show varying levels of [α/Fe], with

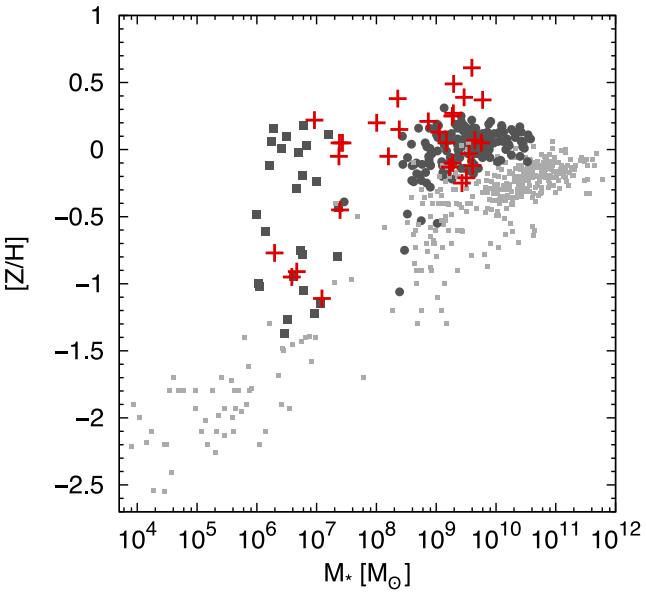

Figure 4. Metallicity versus stellar mass as in Fig. 1. Here the bona-fide galaxies (E/S0s, dEs, and dSphs) are replotted with light grey symbols and our CSSs again with red crosses. In addition, the ATLAS^{3D} galaxies (McDermid et al. 2015) are plotted a second time with stellar mass and metallicity within $R_e/8$ (dark filled circles). The effect of metallicity gradients in massive early-type galaxies can be evaluated, and their inner parts can be compared to the CSSs. The dark filled squares display the dwarf galaxy nuclei of Paudel et al. (2011). The high metallicities of the CSSs are only found in the inner parts of other galaxies.

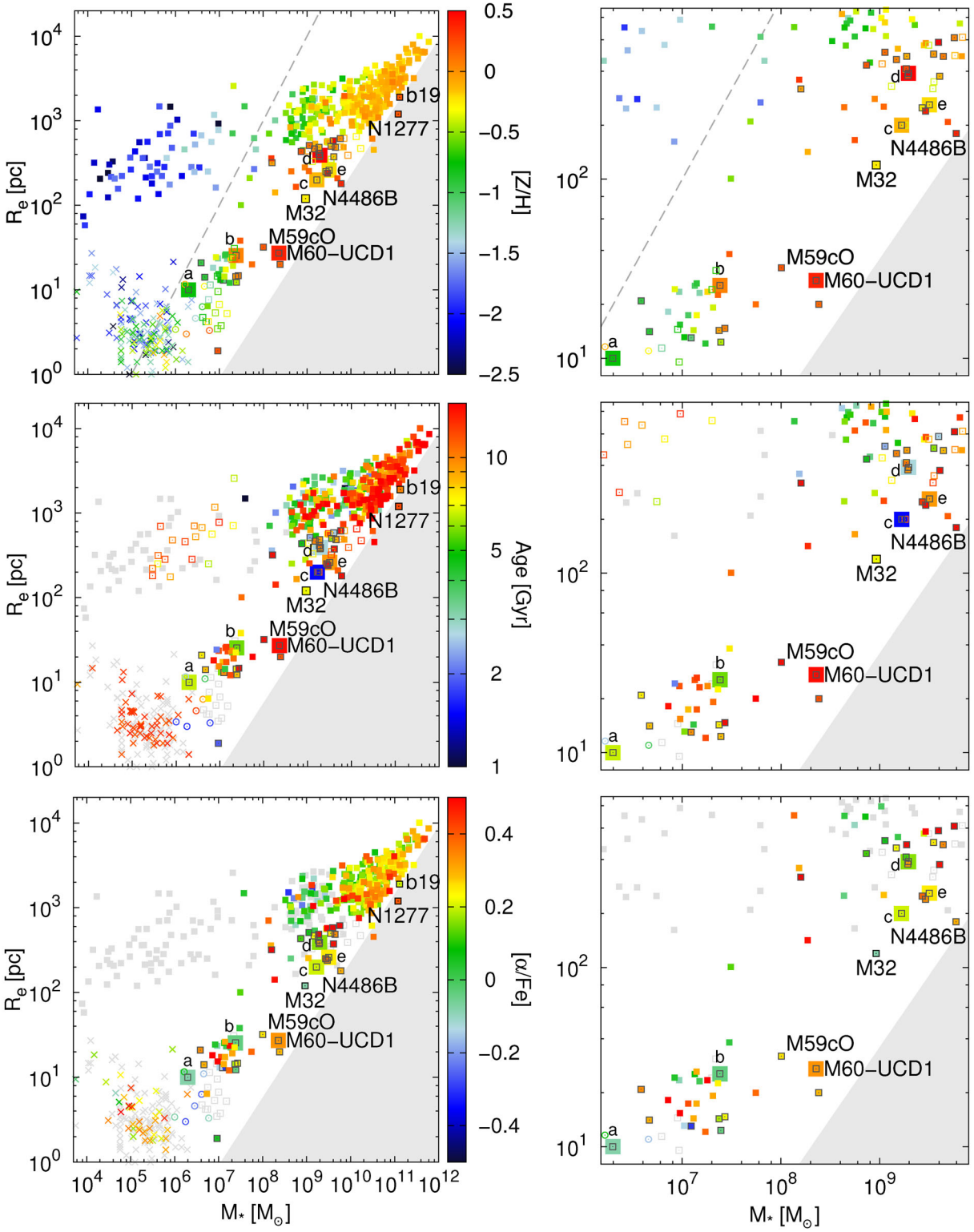

Figure 5. Size–stellar mass plots colour coded by stellar population characteristics. The colours display from top to bottom the SSP-equivalent metallicity, age, and [α/Fe]. The panels in the right-hand column are zoom-ins to the parameter space of our CSSs. GCs are displayed with crosses, dwarf nuclei with open circles, and the rest with squares. Literature CSSs without a measurement of [α/Fe] are shown with open squares. The ages of dSphs are also plotted with open squared, since they are mass-weighted averages, which are upper limits for the luminosity weighted ages. Objects with information lacking are plotted grey. The CSSs (our objects are highlighted with grey borders) exhibit metallicities that exceed those of other objects at the same mass. At low mass a number of them separate from GCs by exhibiting younger ages. The objects discussed in Section 5.1 are highlighted with large symbols (in order of increasing stellar mass: NGC 3628-UCD1 – a, NGC 4546-UCD1 – b, M60-UCD1, VCC 165cE – c, and cE1 and cE2 from Huxor et al. 2011b – d,e). The grey dashed line in the middle panel is a line of constant velocity dispersion inferred from the virial theorem with constant virial coefficient.

Table 2. Basic and stellar population parameters of CSSs.

Name	$M_*(M_\odot)$	R_e(pc)	D (Mpc)	V (km s^{-1})	Age (Gyr)	[Z/H]	[α/Fe]
NGC 4486B	6.0×10^9	180	16.4	1509	$14.5^{+0.4}_{-0.4}$	0.37 ± 0.02	0.30 ± 0.04
PGC 038205[a]	5.7×10^9	616	76.6	6335	$14.5^{+0.9}_{-0.9}$	0.05 ± 0.03	0.50 ± 0.03
NGC 1128cE	4.4×10^9	484	100.0	7603	$8.5^{+2.2}_{-1.7}$	0.07 ± 0.07	0.34 ± 0.09
NGC 2832cE	4.1×10^9	375	98.6	6841	$14.3^{+2.1}_{-1.8}$	−0.12 ± 0.20	0.48 ± 0.17
NGC 2892cE	3.9×10^9	580	97.7	6802	$2.6^{+0.8}_{-0.6}$	0.61 ± 0.09	0.50 ± 0.06
cE0	3.5×10^9	499	85.5	5844	$6.0^{+1.9}_{-1.4}$	−0.03 ± 0.11	0.25 ± 0.11
cE2	3.2×10^9	260	108.1	7580	$9.3^{+5.4}_{-3.4}$	−0.21 ± 0.20	0.25 ± 0.10
NGC 5846cE	2.9×10^9	240	26.7	1479	$14.5^{+1.4}_{-1.3}$	0.39 ± 0.03	0.34 ± 0.04
J233829.31+270225.1	2.7×10^9	250	134.3	9968	$12.6^{+2.8}_{-2.3}$	−0.25 ± 0.07	0.38 ± 0.12
cE1	2.0×10^9	390	92.0	6391	$2.8^{+0.4}_{-0.3}$	0.49 ± 0.06	0.16 ± 0.04
SDSS J075140.40+501102.6	1.9×10^9	485	87.1	6174	$9.2^{+2.9}_{-2.2}$	−0.10 ± 0.10	0.49 ± 0.12
2MASX J01491447+1301548	1.9×10^9	414	71.1	4861	$7.9^{+1.4}_{-1.2}$	0.25 ± 0.06	0.12 ± 0.03
NGC 1272cE	1.9×10^9	377	76.2	3693	$9.5^{+1.2}_{-1.1}$	0.27 ± 0.05	0.32 ± 0.04
VCC 165cE	1.7×10^9	200	180.0	12694	$1.5^{+0.4}_{-0.3}$	−0.13 ± 0.16	0.20 ± 0.12
CGCG 036-042	1.5×10^9	465	32.5	2062	$10.0^{+2.2}_{-1.8}$	0.05 ± 0.08	0.22 ± 0.05
2MASX J16053723+1424418	1.1×10^9	511	67.9	4833	$2.4^{+0.2}_{-0.2}$	0.13 ± 0.05	0.06 ± 0.04
SDSS J133842.45+311457.0	7.4×10^8	433	71.1	4604	$4.6^{+1.8}_{-1.3}$	0.21 ± 0.12	0.12 ± 0.06
M59-UCD3	2.4×10^8	20	14.9	429	$11.7^{+3.0}_{-2.4}$	0.15 ± 0.10	0.29 ± 0.05
M60-UCD2	2.4×10^7	14	16.4	791	$7.6^{+3.9}_{-2.6}$	−0.05 ± 0.13	0.18 ± 0.10
M60-UCD1	2.3×10^8	27	16.4	1278	$14.5^{+3.7}_{-3.0}$	0.38 ± 0.07	0.33 ± 0.04
M59cO	1.0×10^8	32	14.9	723	$14.5^{+4.6}_{-3.5}$	0.20 ± 0.20	0.26 ± 0.10
Sombrero-UCD1	2.7×10^7	14	9.0	1327	$14.5^{+1.7}_{-1.5}$	0.05 ± 0.05	0.22 ± 0.04
NGC 3923-UCD1	2.5×10^7	12	21.3	2135	$8.3^{+1.9}_{-1.6}$	−0.45 ± 0.09	−0.04 ± 0.06
NGC 4546-UCD1	2.4×10^7	25	13.1	1210	$5.8^{+0.1}_{-0.1}$	0.05 ± 0.01	−0.04 ± 0.02
NGC 3923-UCD2	1.2×10^7	13	21.3	1494	$9.5^{+2.4}_{-1.9}$	−1.11 ± 0.14	−0.30 ± 0.19
M85-HCC1	9.2×10^6	1.9	17.9	699	$1.9^{+1.4}_{-0.8}$	0.22 ± 0.15	0.05 ± 0.11
NGC 3923-UCD3	4.6×10^6	14	21.3	2322	$8.3^{+3.3}_{-2.4}$	−0.91 ± 0.16	0.30 ± 0.20
S999	3.8×10^6	20	16.8	1504	$7.6^{+2.0}_{-1.6}$	−0.95 ± 0.12	0.34 ± 0.10
NGC 3628-UCD1	2.0×10^6	10	10.6	824	$6.6^{+1.4}_{-1.2}$	−0.77 ± 0.16	−0.08 ± 0.15

Notes. The distance gives the distance assumed in this work, which is in some cases based on the Hubble flow due to the lack of direct measurements (H_0 = 68 km s^{-1} Mpc^{-1}). The uncertainties of the recession velocities estimated from the Monte Carlo simulations are smaller than 10 km s^{-1} so that they are dominated by the systematics. The stellar population parameters are SSP equivalents. The uncertainties in the stellar population parameters are from the Monte Carlo simulations of the whole index measurement and χ^2-minimization process based on the error spectra (see text). [a]For this object the GALFIT measurement of the size failed, so aperture photometry was done instead. The value for the radius is to be taken with caution due to the bright halo of the host galaxy.

some of them reaching the [α/Fe] of massive galaxies, others being moderately enhanced similar to GCs, and yet others having solar [α/Fe].

5.1 CSSs likely formed by stripping

There is good evidence that six of our CSSs were formed via stripping, and we discuss them below. These objects (NGC 3628-UCD1 – *a*, NGC 4546-UCD1 – *b*, M60-UCD1, VCC 165cE – *c*, cE1 – *d*, cE2 – *e*) are also highlighted in Fig. 5, where stellar age, metallicity, and [α/Fe] are shown as a parameter in the size stellar mass plane. Two of the six objects have supersolar metallicity, and all of them are at least 0.3 dex more metal rich than more diffuse galaxies at similar stellar mass. Two of the stripped high-mass CSSs (cE1 and VCC 165cE) show young ages (<3 Gyr). At low stellar mass, two of the stripped CSSs (NGC 3628-UCD1 and NGC 4546-UCD1) are younger in comparison to the Galactic GCs. While most of the Galactic GCs are α-enhanced, two of the three low-mass stripped CSSs (NGC 3628-UCD1 and NGC 4546-UCD1) show [α/Fe] close to solar or below.

5.1.1 NGC 3628-UCD1

Jennings et al. (2015) described NGC 3628-UCD1 (*a* in Fig. 5) as an ωCen-like object caught in formation via tidal stripping, as it is found within a stellar stream of material of a progenitor object that has been torn apart by NGC 3628. This object is one of those that were observed twice. Both the ESI and MODS spectra result in very consistent age, metallicity, and [α/Fe]. The metallicity ([Z/H] = −0.77 dex) is moderate in comparison to other CSSs, and brings NGC 3628-UCD1 closer to the galaxy mass–metallicity relation. Compared to GCs, the intermediate age and (sub-) solar [α/Fe] set the object apart, consistent with the formation via stripping instead of a GC-type object.

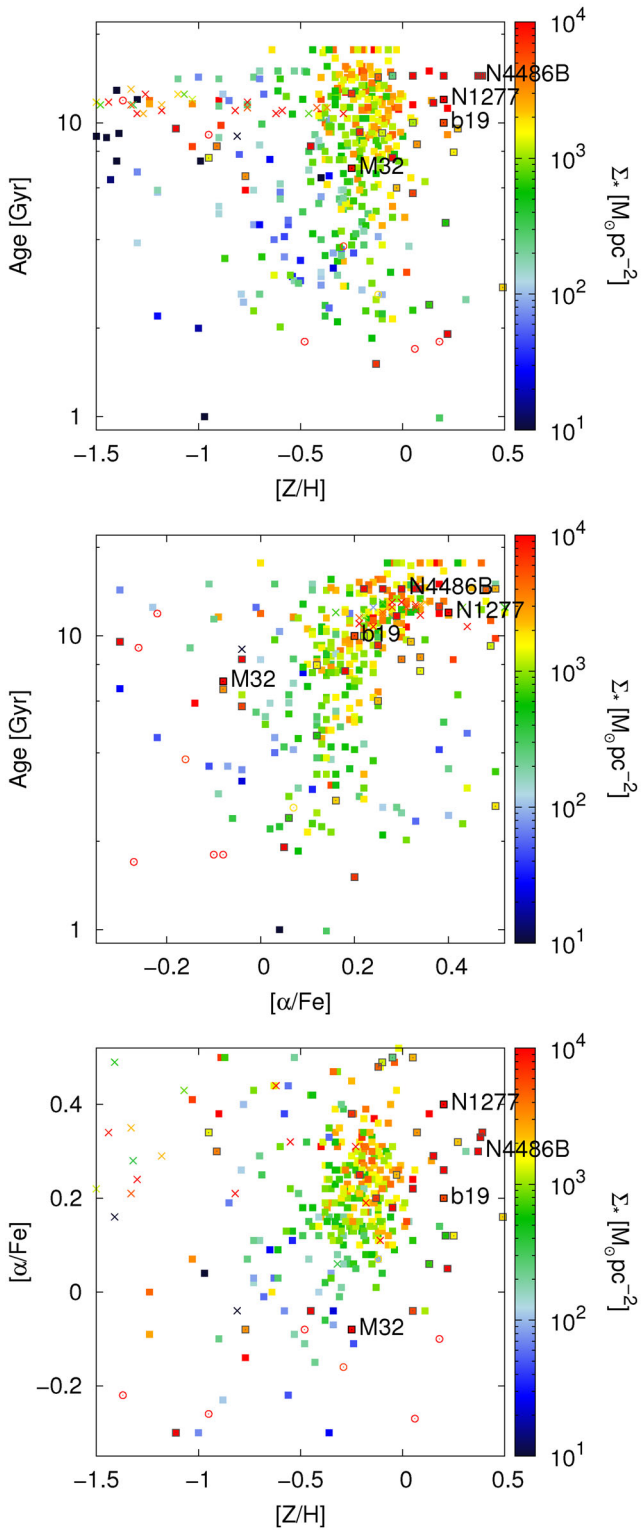

Figure 6. From top to bottom: Age versus metallicity, age versus [α/Fe], and [α/Fe] versus metallicity diagrams. The colours display the average surface density within R_e, $\Sigma_* = M_*/2\pi \times R_e^{-2}$. GCs are displayed with crosses, dwarf nuclei with open circles, and the remaining objects with squares.

5.1.2 *NGC 4546-UCD1*

Using full spectral fitting of a high S/N spectrum of NGC 4546-UCD1 (*b* in Fig. 5) Norris et al. (2015, using the same spectrum as examined here) found that this object was actively forming stars from early epochs until quite recently. This prolonged star formation is unexpected for a star cluster and, taken together with the observation that this object counterrotates its host galaxy, indicates that the object was once the nucleus of a dwarf galaxy that was stripped by NGC 4546 relatively recently. Despite using the same spectrum and similar stellar population models, the luminosity weighted age and metallicities we derive here for NGC 4546-UCD1 are slightly inconsistent with those of Norris et al. (2015, age of 5.8 ± 0.1 versus $4.0^{+0.93}_{-0.75}$ Gyr, $[Z/H] = 0.05 \pm 0.01$ versus 0.18 ± 0.06 dex), difficulty of achieving consistent stellar population parameters when even slightly different analysis codes or models are used. Nevertheless our measurements confirm that NGC 4546-UCD1 is relatively young and metal rich, at least compared to the vast majority of GCs, and furthermore has near solar [α/Fe]. This last fact is expected given the observation that NGC 4546-UCD1 had an extended SFH (Norris et al. 2015).

5.1.3 *M60-UCD1*

Seth et al. (2014) identified a supermassive central black hole in M60-UCD1, which accounts for a disproportionately high fraction of the object's total mass. This is taken as evidence of originating from a more massive galaxy. In contrast to the other objects in this category, M60-UCD1 has a very old age. Like the overly massive black hole, the extremely high metallicity suggests that the object was more massive in its past. Our stellar population parameters are consistent with Strader et al. (2013), who reported solar iron abundances, old age (14.5 ± 0.5 Gyr), and supersolar [α/Fe] $\sim$ +0.2 dex.

5.1.4 *VCC 165cE*

Paudel et al. (2013) described a compact source close to VCC 165 as a background AGN. However, the current SDSS spectrum (Ahn et al. 2014) reveals that VCC 165 has a recession velocity exceeding 12 000 km s^{-1} and close to that of the compact object in its vicinity. While the old velocity measurement of 255 km s^{-1} (NED) placed VCC 165 in the Virgo cluster, like the NGC 4216 system analysed by Paudel et al. (2013), the new value puts it behind the Virgo cluster together with the compact object. The stream connecting the two objects is clearly visible in the NGVS image of Paudel et al. (2013) and likely belongs to this system in the background. Therefore, the compact object should be considered as a cE in formation, and we called it VCC 165cE. The stellar population parameters with a young age ($1.5^{+0.4}_{-0.3}$ Gyr), metallicity around solar ($[Z/H] = -0.13 \pm 0.16$), and $[\alpha/Fe] = 0.20 \pm 0.12$ fit very well to this scenario.

5.1.5 *cE1 and cE2*

Huxor et al. (2011b) discovered two cEs embedded in tidal streams. For cE1 (*d* in Fig. 5) our results and their analysis based on the SDSS spectrum agree qualitatively: young to intermediate age, supersolar metallicity, and slightly enhanced [α/Fe]. Here we obtain a somewhat younger age and higher metallicity. For the age of cE2 (*e* in Fig. 5), the agreement is less good. The analysis of the MODS spectrum suggests that the object is dominated by old stars, unlike the intermediate age of 5.4 ± 1.6 Gyr found by Huxor et al.

(2011b). In order to further investigate the difference, we analysed also the SDSS spectrum. The SDSS spectrum has an S/N of 8–15, while our MODS spectrum has 30–50. For the SDSS spectrum the two different sets of indices (see appendix) yield different ages. The full index set results in an age similar to the one obtained with the MODS spectrum. Only when using the minimal set (Hβ, Mgb, Fe5270, and Fe5335) do we also obtain an intermediate age.

5.1.6 Other candidate stripped CSSs

We note that nine additional cEs were observed to be embedded in tidal streams (Chilingarian et al. 2009; Chilingarian & Zolotukhin 2015), and should be considered as examples with strong direct evidence for a stripping origin.

We also note that the newly discovered object M59-UCD3 (Sandoval et al. 2015) probably fits in this category, since its measured properties make it a virtual clone of M60-UCD1; its stellar mass (2.4 versus 2.3 $\times 10^8$ M$_\odot$), size (20 versus 27 pc), and most importantly its extremely high velocity dispersion ($\sim$70 km s^{-1} from our MODS spectrum versus 68 $\pm$ 5 km s^{-1}; Strader et al. 2013) mean that this object is very likely to host a supermassive black hole like M60-UCD1. Our two spectra (from MODS and ESI) result in consistent stellar population parameters, which are also consistent within the uncertainties with the analyses of Sandoval et al. (2015) and Liu et al. (2015a). The latter study reported a slightly higher velocity dispersion of 78 km s^{-1}. Similar to M60-UCD1, M59-UCD3 also has supersolar metallicity and [α/Fe].

S999, while not featuring a very high metallicity, may also fall into the category of stripped objects. Haşegan et al. (2005) found an extremely high mass-to-light ratio for S999, which was recently confirmed by Janz et al. (2015). The latter study also analysed the stellar populations of S999, and argued that the stars alone (in dynamical equilibrium) cannot account for the mass-to-light ratio. The authors concluded that the apparently too high dynamical mass probably relates to a tidal stripping event. The moderate metallicity of S999 ([Z/H] $= -0.95 \pm 0.12$) shows that excessive amounts of metals may be seen as sufficient for suggesting stripping formation but not absolutely necessary.

6 DISCUSSION

For CSSs of all masses it has been suggested that stripping of originally more massive galaxies is (at least) one formation channel (e.g. Faber 1973; Bekki et al. 2001; Pfeffer & Baumgardt 2013; Norris et al. 2014). The following observations are the key for this idea: CSSs are prevailingly found in environments with high galaxy density and proximity to more massive galaxies, their velocity dispersions are more akin to more massive galaxies than to more diffuse galaxies at fixed stellar mass (e.g. Chilingarian et al. 2009). The latter also applies to the CSS metallicities, which exceed those of galaxies at the same stellar mass.

Here we confirm this for a sample of CSSs spanning a large range in stellar mass, and find generally high metallicities (Fig. 3). Indeed, the metallicities are *too high* when compared to the mass metallicity relation, which is beautifully traced over many orders of magnitudes in stellar mass by our comparison samples. When comparing the metallicity values for the various objects, the details of the measurements have to be considered. For our measurements the value is representative for the stellar population of the entire object, due to the small angular scale and the seeing. The situation is definitely different for the large early-type galaxies, as can be seen in Fig. 3, where the ATLAS^{3D} are plotted twice. The metallicity gradients make the inner parts substantially more metal rich than the stars in the outskirts. Indeed, the extremely high metallicities are only paralleled in the inner parts of more massive galaxies ($R_e/8$ and the mass within this radius of the ATLAS^{3D} galaxies happen to match those of the cEs quite closely). This can be confirmed by comparison to the mass metallicity relation of massive early-type galaxies as traced by SDSS (Gallazzi et al. 2006; Thomas et al. 2010), which is shifted to higher metallicities in comparison to the ATLAS^{3D} relation. Those reach supersolar metallicities, since the small fibre of the spectrograph selects the stars in the galaxies' central regions. The mass–metallicity relation of Thomas et al. (2005) using the metallicities of early-type galaxies within $R_e/10$ passes through the points for the inner parts of the ATLAS^{3D} galaxies in Fig. 4. The stripping scenario suggests that the resulting objects are outliers in the mass–metallicity relation (see also Chilingarian et al. 2009). The progenitor galaxy follows the mass–metallicity relation. The stripping event reduces the stellar mass. However, the stellar metallicity is not reduced, but remains unchanged or can even be enhanced. Two things can play a role: first, preferentially stars in the outer parts with lower metallicity will be stripped, leading to higher averaged values. Secondly, the interaction cannot only lead to the stripping of stars, but also to gas inflows to the centre where a starburst enabled additional enrichment (e.g. for gas-rich progenitors – as for example was suggested for M32 Graham 2002 – see also Forbes et al. 2003). This possibly can also alleviate an apparent lack of progenitors for the very metal richest CSSs

6.1 Stripping at work

Several discoveries of CSSs caught in the act of formation via stripping (e.g. Chilingarian et al. 2009; Huxor et al. 2011b; Chilingarian & Zolotukhin 2015; Jennings et al. 2015) undoubtedly tell us that stripping contributes to the population of CSSs. As seen in Section 5.1 these 'smoking gun' examples share the characteristic of exceedingly high metallicity when compared to the mass–metallicity relation. This supports the idea that the stripping scenario is a viable option for a large number of CSSs which have also metallicities in excess of the expectation from the mass–metallicity relation. The objects in Section 5.1 are mostly of relatively young age, which seems to be different from the conventional wisdom of an old age of UCDs and cEs. However, there is a selection effect in play, since the evidence for a stripping origin for both the detection of tidal streams and extended SFHs disfavour purely old age. The detection of tidal streams sets a limit on the age since the interaction, since these features are rather short lived (e.g. Rudick et al. 2009). When some boost of star formation accompanies the stripping event (e.g. Forbes et al. 2003; Emsellem & van de Ven 2008) these objects with tidal features are expected to have young average ages. Likewise extended SFHs mean that there are younger stars present, which contribute overproportionally to the light, so that the luminosity weighted SSP-equivalent age cannot be very old.

M60-UCD1 is an exception to this. In this case, the (exceedingly high) mass of the central black hole suggests a stripping origin (Seth et al. 2014). Unlike tidal streams, the black hole can be detected and its mass measured also long after the stripping event. Also, there are several cEs known to host central massive black holes (e.g. NGC 4486B, M32; Kormendy et al. 1997; van den Marel et al. 1997; NGC 5846A has central kinematics very similar to NGC 4486B based on the spectra with high spatial resolution of Davidge, Beck & McGregor 2008), which are too massive when comparing

to the black hole mass spheroid mass relation (e.g. Magorrian et al. 1998, for M32 it can be discussed whether it follows the relation, or whether its very well measured black hole mass unduly affects and, therefore, biases the relation). Overly massive black holes can be interpreted as evidences that the CSSs were more massive at an earlier time (just like the exceedingly high metallicities), and that a stripping event reduced their stellar mass to the observed amount.

6.2 Isolated cEs

Interestingly, one of the two isolated CSSs (CGCG 036-042; Paudel et al. 2014) has a low metallicity compared to the bulk of our CSSs, which places it within the scatter of the galaxy mass–metallicity relation (albeit as an extreme case). The other isolated cE in our sample (cE0; Huxor et al. 2013), has around solar metallicity. While the results for metallicity and [α/Fe] are consistent within the uncertainties, there is some tension for the age, with the age derived from the MODS spectrum being younger than the Huxor et al. (2013) value based on the SDSS spectrum, which has a slightly higher S/N of 18–27. We reanalysed the SDSS spectrum and find an age consistent with that of Huxor et al. (2013). The value we use throughout the paper is the weighted average, consistently with other objects that have multiple spectra. This value is consistent within the uncertainties with Huxor et al. (2013).

Chilingarian & Zolotukhin (2015) did not find any statistically significant difference between isolated and other cEs. Chilingarian & Zolotukhin concluded that the isolated cE formed in high density regions and then escaped, avoiding the need for an alternative formation scenario for the rare isolated cases (Huxor et al. 2013; Paudel et al. 2014).

6.3 GCs, UCDs, and the mass range $\sim 10^6$–10^8 $M_\odot$

In the mass range $\sim 10^6$–10^8 $M_\odot$ CSSs formed by stripping are joined with the high-mass end of GCs, and it has been suggested that UCDs are simply large GCs (e.g. Fellhauer & Kroupa 2002; Mieske et al. 2013). Recent literature provides evidence that both formation channels, i.e. stripping and large GCs, operate at the low-mass end of the CSS population (AIMSS I; Hilker 2006; Brodie et al. 2011; Chiboucas et al. 2011; Chilingarian et al. 2011; Da Rocha et al. 2011; Norris & Kannappan 2011; Pfeffer et al. 2014). Consistent with this mixed scenario, we observe a wide range of metallicities and old, as well as intermediate, ages of our CSSs at low mass.

The stellar population characteristics actually can help to tell the stripped objects and star clusters apart. Norris et al. (2015) analysed two of the objects in detail, benefiting from very high quality spectra, and they were able to constrain the SFHs of the objects. While NGC 3923-UCD1 basically has only old stars and fits readily into the star cluster category, NGC 4546-UCD1 has a SFH extending to the recent past when the progenitor was stripped (see also Norris & Kannappan 2011). Several other CSSs with similar mass have solar [α/Fe], including the stripped objects NGC 4546-UCD1 and NGC 3628-UCD1. This could hint at longer lasting star formation episodes (e.g. Norris & Kannappan 2011; Norris et al. 2015), and it is different from the generally α-enhanced Milky Way GCs (Pritzl et al. 2005). Evstigneeva et al. (2008) noted that the reverse is not necessarily valid, since early stripping can lead to α-enhanced UCDs.

In our sample it appears as if there is a gap in mass between UCDs and GCs. However, this is a selection effect, due to combining (extragalactic) UCDs bright enough to obtain spectroscopy with Milky Way GCs. Generally, there is an overlap in mass of UCDs and the GC systems of galaxies, and the possibility of UCDs following the GC luminosity function was one reason for relating the two (Hilker 2006; Norris & Kannappan 2011; Mieske et al. 2012).

When comparing to the metallicity distribution of the extragalactic GCs from Usher et al. (2012), it needs to be considered that their sample also contains bright objects, which are more massive than ωCen, since they did not impose an upper limit in luminosity. Of the objects in Usher et al. (2012) 10.8 per cent have supersolar metallicities and 6.0 per cent have [Z/H] > 0.2. When only counting those that have 1σ larger metallicities than the limits, the fraction reduces to 2.8 and 1.0 per cent, respectively. Some of those massive objects may be stripped nuclei like NGC 3628-UCD1, and should be classified as UCDs. Furthermore, it can be expected that none of our CSSs are a GC-type of object with very low metallicity ([Z/H] < -1.5). Being restricted to high stellar masses in terms of GCs means that any GC-like object in the sample is expected to be affected by the blue tilt, i.e. should have managed to increase its metallicity due to self-enrichment (e.g. Norris & Kannappan 2011).

We note that young massive star clusters (YMCs) in the local Universe reach densities similar to those of the CSSs and typically have around solar or even supersolar metallicities (e.g. Schweizer & Seitzer 1998; Maraston et al. 2001, 2004; Strader et al. 2003; Bastian et al. 2013). The high metallicities are not surprising in this case, since YMCs are forming from gas in merging spiral galaxies at redshift $z = 0$. However, this also dictates their very young age. Evolved YMCs may contribute to the population of low-mass CSSs, but seem to be an unlikely option for the old CSSs with highest metallicity.

The more massive CSSs do not span a metallicity range as large as at low mass, and they are all more metal rich than [Z/H] > -0.5. Norris & Kannappan (2011) used the GC luminosity function to estimate the highest GC mass expected in the most populous GC systems. Based on this, no object more massive than a few times 10^7 $M_\odot$ can be a GC. Interestingly, the CSSs in our sample are exclusively metal rich above a similar mass scale (cf. Fig. 3).

The dwarf nuclei of Paudel et al. (2010a), as objects potentially being liberated by stripping to form CSSs, seem to mostly be restricted to sub-solar to at most solar metallicities and [α/Fe] in Fig. 5. When considering their full sample, however, this appears to be a bias effect (see also Fig. 3) introduced by restricting our sample to those objects with measured sizes (from Côté et al. 2006). In their complete sample there are a number of nuclei with slightly supersolar metallicities and/or enhanced [α/Fe]. Paudel et al. (2010a) stated that the dwarf nuclei of those dEs, which are located in regions with the same high local projected galaxy density as UCDs, share similar characteristics with those. This is possibly related to a trend of stripping being less effective in clusters at later times (Pfeffer et al. 2014), and threshed nuclei, as well as nucleated dwarfs with their star formation ceased long ago, having the tendency to be located towards the centre of the cluster.

Francis et al. (2012) studied a sample of Virgo (including some UCDs also present in Paudel et al.) and Fornax cluster UCDs. Their analysis found also a large spread in metallicities, and mostly old age and supersolar [α/Fe]. Francis et al. concluded that the metallicity and age distributions are different from present day nucleated dEs, and that the one cannot transform into the other by stripping. Instead, they stated that the UCD metallicity distribution is similar to that of the GCs, with the UCDs not conforming to a metallicity–luminosity relation. Brodie et al. (2011), on the other hand, described the UCD colour–magnitude relation as closely linked to that of dwarf nuclei, and concluded that the two are likely interrelated. In Fig. 3, we show that the Paudel et al. (2010a) sample

of nuclei, which were carefully separated from their host galaxies, span the complete metallicity range of the UCDs. Our sample of UCDs contains also some that are younger than classical GCs, as well as objects with solar [α/Fe] (Fig. 5), so that the UCD stellar populations are overall not same as those in GCs. Moreover, we identified a transition mass, above which the objects are exclusively metal rich, and are not expected to be GCs. In the context of comparing UCDs with GC and dE nuclei, it is also noteworthy that Liu et al. (2015b) found a continuum from UCDs to UCDs with envelopes to dEs with nuclei, and Zhang et al. (2015) reported that the spatial distribution of UCDs around M87 and their velocities distribution are distinct from those of the GC system. Both studies concluded that the UCDs are not exclusively massive GCs.

Additional evidence for a contribution to the CSS population by stripping in this mass range was found by Forbes et al. (2014), who measured dynamical masses exceeding the stellar mass significantly (see also Taylor et al. 2015). They also showed that this enhancement of dynamical mass was a good fit to the stripping simulations of Pfeffer & Baumgardt (2013). One of these objects with an extreme mass ratio is S999 (Haşegan et al. 2005; Janz et al. 2015), which does not have a very high metallicity ([Z/H] $-$ 0.95). In the picture of UCDs being surviving nuclei of stripped dwarf galaxies there is a reservoir of nuclei with matching low metallicity. Furthermore, the simulations of Pfeffer & Baumgardt (2013) suggest that the remnants can become as small and as low-mass as GCs.

6.4 Compact ellipticals and the mass range of $\sim 10^8$–10^{10} M$_\odot$

At higher masses of $\sim 10^8$–10^{10} M$_\odot$, the high metallicities (in comparison to the general mass–metallicity relation) potentially indicate that the objects were more massive galaxies in their past, and only later reduced in mass by stripping of material (see also e.g. Chilingarian et al. 2009). The two of our objects that have been observed to feature tidal tails (Huxor et al. 2011b) strengthen this scenario. One of the objects is comparably young, which may be expected if stars were formed in, or up until, the interaction, which happened rather recently. There are nine additional cEs known to be embedded in tidal streams (Chilingarian et al. 2009; Chilingarian & Zolotukhin 2015). These objects show a range of age (6.3 Gyr and older), with four of them being older than 10 Gyr. Their metallicities are generally high ($-0.34 \leq$ [Fe/H] ≤ 0.12), with most of them being around solar and higher. In particular, the latest study (Chilingarian & Zolotukhin 2015) increases the number of cEs in tidal streams substantially, thereby amplifying the mounting evidence for cE formation via tidal stripping. Additional evidence for a past as a more massive galaxy includes overly massive central black holes, such as NGC 4486B, in which the black hole contributes 11 per cent to the total mass – much more than the 0.1 per cent expected from the black hole bulge mass scaling relation (Magorrian et al. 1998). Sometimes, also a two-component structure, such as that seen in M32 (Graham 2002), was taken as evidence of a stripped disc.

Several of the high-mass CSSs in the literature have more normal metallicities, i.e. sub-solar. For some of them [α/Fe] was not measured. Thus the comparison might not be entirely fair, since including [α/Fe] in the metal budget can bias the metallicity result to higher values. The other three low metallicity cEs are in the Virgo cluster and they represent the least compact objects in the sample of Guérou et al. (2015). Their size is large enough that they may potentially be regarded as small *normal* dEs.

At even higher masses there are some compact galaxies that have recently acquired a lot of attention. They have very high velocity dispersions for their luminosity, and they are close to or even within the *zone of avoidance* (Fig. 1). van den Bosch et al. (2012) claimed that NGC 1277 also has an overly massive central black hole, with the most extreme value for the mass contribution of the black hole at 59 per cent of the bulge mass. While Läsker et al. (2013) do not have definite proof for an overly massive black hole in J151741.75−004217.6 or b19, they consider it likely.

These objects also share very high metallicities with our CSSs. There are also potentially more of these kinds of objects (Saulder, van den Bosch & Mieske 2015). While the characteristics of high metallicity and overly massive black holes could inspire similar ideas for their formation, their origin is thought to be different. In part this is due to a lack of potential hosts to cause the stripping. Instead, it has been suggested that they constitute descendants of compact galaxies at high redshift, so-called *red nuggets* (van der Wel et al. 2014). In this context, it is very interesting that recently Lonoce et al. (2015) measured a very high metallicity ([Z/H] > 0.5) for an early-type galaxy at redshift $z \sim 1.4$. While unevolved red nuggets may be expected to have very old ages, unlike some of our CSSs, it is beyond the scope of this paper to explore whether the formation channels for red nuggets are a possibility for some other of CSSs (cf. also Graham, Dullo & Savorgnan 2015). However, the possibility reminds us that stripping is not necessarily the only formation mechanism for CSSs, and some of them may in a sense be the *true continuation* of ellipticals towards lower mass (e.g. Kormendy et al. 2009).

6.5 Enrichment and escape velocity

It is unclear whether the mass–metallicity relation is caused by a primary dependence of metallicity on mass, or whether it is a consequence of fundamental relationships between other quantities, such as velocity dispersion or escape velocity (e.g. Davies, Sadler & Peletier 1993; Bernardi et al. 2003), which are also related to mass. In Fig. 5, lines with constant velocity dispersions, assuming the virial theorem and constant virial coefficient, run somewhat steeper than the border of the zone of avoidance. The metallicities of all objects overall seem to trace velocity dispersion much more closely than stellar mass (cf. Guérou et al. 2015). In Fig. 6, the parameter space spanned by age, metallicity, and [α/Fe] is shown with the colours of the symbols displaying the effective stellar surface density within R_e. Systematic trends in these plots suggest higher dimensional relations of the parameters involved (e.g. Brodie et al. 2011; Guérou et al. 2015; Sandoval et al. 2015). Instead of exploring those in depth, we focus in the following on relations with escape velocity.

Scott et al. (2009, 2013) made use of dynamical modelling and metallicity maps from the Spectroscopic Areal Unit for Research on Optical Nebulae (SAURON) integral-field unit (IFU) to show that metallicity and escape velocity are related locally within the galaxies for a substantial sample of early-type galaxies. Especially when using Mgb as a proxy for metallicity, they found a very tight relation. Moreover, the authors discovered that their early-type galaxies span a plane in the four-dimensional space of escape velocity and SSP-equivalent stellar population parameters age, metallicity, and [α/Fe]. Again, this is also true for the local escape velocity and stellar population characteristics.

For our CSSs, spatially resolved spectroscopy, needed for dynamical modelling and determination of stellar population parameters locally, is unavailable. Instead, we compare their global parameters to the findings of Scott et al. (2009, 2013) in Fig. 7. For the escape velocity we use two different methods, which are designed to be lower and upper limits. The stellar population parameters from

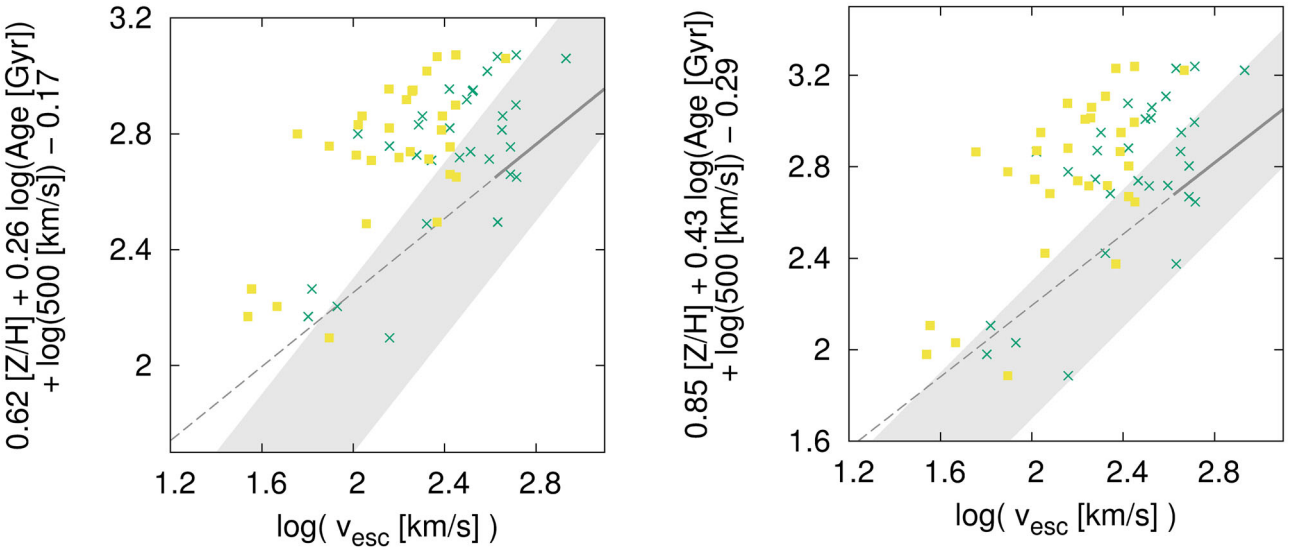

Figure 7. SSP-equivalent stellar population parameters and escape velocity. The two panels show the edge-on projections of the planes that Scott et al. (2013, left) and Scott et al. (2009, right) found to be spanned by the local stellar population parameters and escape velocities in early-type galaxies. The grey shaded regions indicate these planes ±0.3 dex, which is chosen by eye to generously describe regions that were populated by the profiles in these studies. For our CSSs, we calculate the corresponding linear combinations of luminosity weighted age and metallicities and lower (yellow boxes) and upper (green crosses) limits for the luminosity weighted escape velocities (see text). The grey lines indicate the relations found by Scott et al. (2013) and Scott et al. (2009) for escape velocities above 400 km s^{-1}, where the authors found the scatter to be considerably smaller. The CSSs fall on average well above the planes and relations for early-type galaxies, suggesting that their enrichments exceed what is possible for their current potential wells.

the spectra are light-weighted averages. In order to find the corresponding light-weighted average escape velocity, we first assume a constant mass-to-light ratio and a Plummer sphere (Plummer 1911) for convenient integration. With the stellar mass and size of the CSSs the value within the projected half-light radius can be readily calculated. However, in particular for the cEs, this will underestimate the real light weighted escape velocity, since their profile is steeper and both light and escape velocity increase towards the centre. Therefore, we calculate as a second method an upper limit by assuming a Dehnen profile (Dehnen 1993) with $\gamma = 3/2$, which approximates the de-projected mass profile for a de Vaucouleurs profile, and find its maximum escape velocity. Note that this should represent a generous upper limit, since we use the maximum escape velocity, and since the majority of CSSs including the cEs have profiles shallower than a de Vaucouleurs profile (which corresponds to a Sérsic profile with an index $n = 4$, while most CSSs have $1 < n < 2.5$).

Fig. 7 illustrates that even for this latter maximum escape velocity the CSSs, and especially the cEs, fall partly beyond the regions traced by the early-type galaxies. This is true for both the area enclosing all the local values of Scott et al. (2009, 2013) and the relations the authors found for escape velocity $v_{\rm esc} > 400$ km s^{-1}, which is even tighter according to them. At lower escape velocity the scatter is increased, mostly by galaxies with negative gradients and central star formation and dust. We include the comparison to both studies, since Scott et al. (2013) pointed out that their sample, although larger, included poorer quality data, so the earlier work might provide a more reliable reference plane. The cEs fall above the relations in both cases. If the local escape velocity indeed determines the effectiveness of the enrichment process, the exceedingly high metallicities of the CSSs (implying $v_{\rm esc} \gtrsim 600$ km s^{-1} using the planes) are a strong indication that those objects were more massive in their past.

7 CONCLUSIONS

We have presented the stellar population characteristics (SSP equivalent age, metallicity, and [α/Fe]) for a sample of 29 CSSs and compared to literature values for CSSs and other types. Many of the CSSs have metallicities that are *too high* when compared to the mass–metallicity relation traced by the comparison sample of early-type galaxies. In fact some of the objects appear to have a metallicity exceeding that of the inner parts (within $R_{\rm e}/8$) of massive early-type galaxies.

At high mass, the departure of the cEs from the galaxy mass–metallicity relation argues against them being a simple continuation of the massive early-type galaxies. In the UCD mass range, we find a transition such that the metallicity distribution of objects less massive than a few times 10^7 M$_\odot$ is wide, similar to that of GCs, while more massive objects are all metal rich. This transition coincides with the mass at which luminosity function arguments previously suggested the GC population ends.

The high metallicities in UCDs and cEs are only paralleled by those of dwarf nuclei and the central parts of massive early types. We interpret these findings as an indication that they were more massive at an earlier time and underwent tidal stripping to obtain their current mass and compact size. This interpretation is supported by the fact that objects with direct evidence for a stripping origin have similarly high metallicities.

Future instrumentation will provide the means to hunt for further clues about the formation histories of CSSs, such as detecting and weighing supermassive central black holes. Other promising avenues include the taxonomy of individual elements in the stellar populations (e.g. Evstigneeva et al. 2007; Taylor et al. 2010; Colucci et al. 2013; Strader et al. 2013) and exploring multidimensional relations between the stellar populations and physical parameters such as mass, size, and compactness as hinted at by Fig. 6 (e.g. Brodie et al. 2011; Guérou et al. 2015; Sandoval et al. 2015).

For now, the integrated stellar population parameters offer valuable clues to the formation history of CSSs, especially since such information is considerably easier to obtain than resolved SFHs or direct measurements of overly massive central black holes. Young age and solar [α/Fe], which are measurable in objects where tidal tails have already faded, can provide evidence to distinguish them from massive star clusters.

Furthermore, we followed the studies of Scott et al. (2009, 2013) in comparing the stellar populations as a function of escape velocity. The authors found massive early-type galaxies to form a plane in a parameter space spanned by the local escape velocity and the local stellar population parameters, i.e. age, metallicity, and [α/Fe]. A plausible explanation could be that the efficiency of enrichment depends locally on the ability to retain metals, as indicated by the escape velocity. The CSSs fall, on average, above these narrow planes found by Scott et al. (2009, 2013), which can be understood as evidence that their current mass is too small for the level of enrichment that the CSSs have reached. This is a strong argument in favour of the stripping scenario, and suggests that metallicity can be utilized to tell apart objects with a more massive past in the transition region of massive objects with sizes of around 500 pc.

ACKNOWLEDGEMENTS

We thank our referee Igor Chilingarian for useful suggestions that helped improving the paper. We thank Carlos Morante for helpful discussions. JJ and DAF thank the ARC for financial support via DP130100388. This work was supported by NSF grants AST-1109878, AST-1515084, and AST-1518294. MJF gratefully acknowledges support from the DFG via Emmy Noether Grant Ko 4161/1.

This paper used data obtained with the MODS spectrographs built with funding from NSF grant AST-9987045 and the NSF Telescope System Instrumentation Program (TSIP), with additional funds from the Ohio Board of Regents and the Ohio State University Office of Research.

The LBT is an international collaboration among institutions in the United States, Italy, and Germany. LBT Corporation partners are: The University of Arizona on behalf of the Arizona university system; Istituto Nazionale di Astrofisica, Italy; LBT Beteiligungsgesellschaft, Germany, representing the Max-Planck Society, the Astrophysical Institute Potsdam, and Heidelberg University; The Ohio State University, and The Research Corporation, on behalf of The University of Notre Dame, University of Minnesota and University of Virginia.

Based on observations obtained at the Gemini Observatory, as part of programmes GS-2011A-Q-13, GS-2013A-Q-26, GS-2014A-Q-30, and processed using the Gemini IRAF package. The Gemini Observatory is operated by the Association of Universities for Research in Astronomy, Inc, under a cooperative agreement with the NSF on behalf of the Gemini partnership: the National Science Foundation (United States), the National Research Council (Canada), CONICYT (Chile), the Australian Research Council (Australia), Ministério da Ciência, Tecnologia e Inovação (Brazil) and Ministerio de Ciencia, Tecnología e Innovación Productiva (Argentina).

Some of the data presented herein were obtained at the W.M. Keck Observatory, which is operated as a scientific partnership among the California Institute of Technology, the University of California and the National Aeronautics and Space Administration. The Observatory was made possible by the generous financial support of the W.M. Keck Foundation.

We wish to recognize and acknowledge the very significant cultural role and reverence that the summit of Mauna Kea has always had within the indigenous Hawaiian community. We are most fortunate to have the opportunity to conduct observations from this mountain.

Funding for SDSS-III has been provided by the Alfred P. Sloan Foundation, the Participating Institutions, the National Science Foundation, and the US Department of Energy Office of Science. The SDSS-III web site is http://www.sdss3.org/.

SDSS-III is managed by the Astrophysical Research Consortium for the Participating Institutions of the SDSS-III Collaboration including the University of Arizona, the Brazilian Participation Group, Brookhaven National Laboratory, Carnegie Mellon University, University of Florida, the French Participation Group, the German Participation Group, Harvard University, the Instituto de Astrofisica de Canarias, the Michigan State/Notre Dame/JINA Participation Group, Johns Hopkins University, Lawrence Berkeley National Laboratory, Max Planck Institute for Astrophysics, Max Planck Institute for Extraterrestrial Physics, New Mexico State University, New York University, Ohio State University, Pennsylvania State University, University of Portsmouth, Princeton University, the Spanish Participation Group, University of Tokyo, University of Utah, Vanderbilt University, University of Virginia, University of Washington, and Yale University.

REFERENCES

Ahn C. P. et al., 2014, ApJS, 211, 17
Bassino L. P., Muzzio J. C., Rabolli M., 1994, ApJ, 431, 634
Bastian N., Schweizer F., Goudfrooij P., Larsen S. S., Kissler-Patig M., 2013, MNRAS, 431, 1252
Bekki K., Couch W. J., 2003, ApJ, 596, L13
Bekki K., Couch W. J., Drinkwater M. J., 2001, ApJ, 552, L105
Bernardi M. et al., 2003, AJ, 125, 1866
Brodie J. P., Romanowsky A. J., Strader J., Forbes D. A., 2011, AJ, 142, 199
Cappellari M., Emsellem E., 2004, PASP, 116, 138
Cappellari M. et al., 2011, MNRAS, 413, 813
Chiboucas K. et al., 2011, ApJ, 737, 86
Chilingarian I., 2009, MNRAS, 394, 1229
Chilingarian I., Zolotukhin I., 2015, Science, 348, 418
Chilingarian I., Cayatte V., Chemin L., Durret F., Laganá T. F., Adami C., Slezak E., 2007, A&A, 466, L21
Chilingarian I. V., Cayatte V., Bergond G., 2008, MNRAS, 390, 906
Chilingarian I., Cayatte V., Revaz Y., Dodonov S., Durand D., Durret F., Micol A., Slezak E., 2009, Science, 326, 1379
Chilingarian I. V., Mieske S., Hilker M., Infante L., 2011, MNRAS, 412, 1627
Choi P. I., Guhathakurta P., Johnston K. V., 2002, AJ, 124, 310
Colucci J. E., Fernanda Durán M., Bernstein R. A., McWilliam A., 2013, ApJ, 773, L36
Côté P. et al., 2006, ApJS, 165, 57
Da Rocha C., Mieske S., Georgiev I. Y., Hilker M., Ziegler B. L., Mendes de Oliveira C., 2011, A&A, 525, A86
Dabringhausen J., Hilker M., Kroupa P., 2008, MNRAS, 386, 864
Davidge T. J., Beck T. L., McGregor P. J., 2008, ApJ, 677, 238
Davies R. L., Sadler E. M., Peletier R. F., 1993, MNRAS, 262, 650
Dehnen W., 1993, MNRAS, 265, 250
Drinkwater M. J., Jones J. B., Gregg M. D., Phillipps S., 2000, PASA, 17, 227
Drinkwater M. J., Gregg M. D., Hilker M., Bekki K., Couch W. J., Ferguson H. C., Jones J. B., Phillipps S., 2003, Nature, 423, 519
Emsellem E., van de Ven G., 2008, ApJ, 674, 653
Evstigneeva E. A., Gregg M. D., Drinkwater M. J., Hilker M., 2007, AJ, 133, 1722

Evstigneeva E. A. et al., 2008, AJ, 136, 461
Faber S. M., 1973, ApJ, 179, 423
Fellhauer M., Kroupa P., 2002, MNRAS, 330, 642
Fellhauer M., Kroupa P., 2005, MNRAS, 359, 223
Forbes D. A., Kroupa P., 2011, PASA, 28, 77
Forbes D. A., Beasley M. A., Bekki K., Brodie J. P., Strader J., 2003, Science, 301, 1217
Forbes D. A., Spitler L. R., Graham A. W., Foster C., Hau G. K. T., Benson A., 2011, MNRAS, 413, 2665
Forbes D. A., Pota V., Usher C., Strader J., Romanowsky A. J., Brodie J. P., Arnold J. A., Spitler L. R., 2013, MNRAS, 435, L6
Forbes D. A., Norris M. A., Strader J., Romanowsky A. J., Pota V., Kannappan S. J., Brodie J. P., Huxor A., 2014, MNRAS, 444, 2993
Foster C. et al., 2014, MNRAS, 442, 3544
Francis K. J., Drinkwater M. J., Chilingarian I. V., Bolt A. M., Firth P., 2012, MNRAS, 425, 325
Gallazzi A., Charlot S., Brinchmann J., White S. D. M., 2006, MNRAS, 370, 1106
Graham A. W., 2002, ApJ, 568, L13
Graham A. W., Dullo B. T., Savorgnan G. A. D., 2015, ApJ, 804, 32
Guérou A. et al., 2015, ApJ, 804, 70
Harris W. E., 1996, AJ, 112, 1487
Haşegan M. et al., 2005, ApJ, 627, 203
Hilker M., 2006, preprint (astro-ph/0605447)
Hilker M., Infante L., Vieira G., Kissler-Patig M., Richtler T., 1999, A&AS, 134, 75
Hook I. M., Jørgensen I., Allington-Smith J. R., Davies R. L., Metcalfe N., Murowinski R. G., Crampton D., 2004, PASP, 116, 425
Huxor A. P., Phillipps S., Price J., Harniman R., 2011b, MNRAS, 414, 3557
Huxor A. P., Phillipps S., Price J., 2013, MNRAS, 430, 1956
Janz J., Lisker T., 2008, ApJ, 689, L25
Janz J., Lisker T., 2009, ApJ, 696, L102
Janz J., Forbes D. A., Norris M. A., Strader J., Penny S. J., Fagioli M., Romanowsky A. J., 2015, MNRAS, 449, 1716
Jennings Z. G. et al., 2015, ApJ, 812, L10
Kissler-Patig M., Jordán A., Bastian N., 2006, A&A, 448, 1031
Kormendy J. et al., 1997, ApJ, 482, L139
Kormendy J., Fisher D. B., Cornell M. E., Bender R., 2009, ApJS, 182, 216
Läsker R., van den Bosch R. C. E., van de Ven G., Ferreras I., La Barbera F., Vazdekis A., Falcón-Barroso J., 2013, MNRAS, 434, L31
Le Borgne J.-F. et al., 2003, A&A, 402, 433
Liu C. et al., 2015a, ApJ, 812, L2
Liu C. et al., 2015b, ApJ, 812, 34
Lonoce I. et al., 2015, MNRAS, 454, 3912
McConnachie A. W., 2012, AJ, 144, 4
McDermid R. M. et al., 2015, MNRAS, 448, 3484
Magorrian J. et al., 1998, AJ, 115, 2285
Maraston C., 2005, MNRAS, 362, 799
Maraston C., Kissler-Patig M., Brodie J. P., Barmby P., Huchra J. P., 2001, A&A, 370, 176
Maraston C., Bastian N., Saglia R. P., Kissler-Patig M., Schweitzer F., Goudfrooij P., 2003, A&A, 400, 823
Maraston C., Bastian N., Saglia R. P., Kissler-Patig M., Schweizer F., Goudfrooij P., 2004, A&A, 416, 467
Mieske S., Kroupa P., 2008, ApJ, 677, 276
Mieske S., Infante L., Hilker M., Hertling G., Blakeslee J. P., Benítez N., Ford H., Zekser K., 2005, A&A, 430, L25
Mieske S., Dabringhausen J., Kroupa P., Hilker M., Baumgardt H., 2008, Astron. Nachr., 329, 964
Mieske S., Hilker M., Misgeld I., 2012, A&A, 537, A3
Mieske S., Frank M. J., Baumgardt H., Lützgendorf N., Neumayer N., Hilker M., 2013, A&A, 558, A14
Misgeld I., Hilker M., 2011, MNRAS, 414, 3699
Misgeld I., Mieske S., Hilker M., Richtler T., Georgiev I. Y., Schuberth Y., 2011, A&A, 531, A4
Norris M. A., Kannappan S. J., 2011, MNRAS, 414, 739
Norris M. A. et al., 2012, MNRAS, 421, 1485
Norris M. A. et al., 2014, MNRAS, 443, 1151 (AIMSS I)
Norris M. A., Escudero C. G., Faifer F. R., Kannappan S. J., Forte J. C., van den Bosch R. C. E., 2015, MNRAS, 451, 3615
Orban C., Gnedin O. Y., Weisz D. R., Skillman E. D., Dolphin A. E., Holtzman J. A., 2008, ApJ, 686, 1030
Paudel S., Lisker T., Kuntschner H., Grebel E. K., Glatt K., 2010a, MNRAS, 405, 800
Paudel S., Lisker T., Janz J., 2010b, ApJ, 724, L64
Paudel S., Lisker T., Kuntschner H., 2011, MNRAS, 413, 1764
Paudel S. et al., 2013, ApJ, 767, 133
Paudel S., Lisker T., Hansson K. S. A., Huxor A. P., 2014, MNRAS, 443, 446
Pfeffer J., Baumgardt H., 2013, MNRAS, 433, 1997
Pfeffer J., Griffen B. F., Baumgardt H., Hilker M., 2014, MNRAS, 444, 3670
Plummer H. C., 1911, MNRAS, 71, 460
Pogge R. W. et al., 2010, in McLean I. S., Ramsay S. K., Takami H., eds, Proc. SPIE Conf. Ser. Vol. 7735, Ground-based and Airborne Instrumentation for Astronomy III. SPIE, Bellingham, p. 77350A
Price J. et al., 2009, MNRAS, 397, 1816
Pritzl B. J., Venn K. A., Irwin M., 2005, AJ, 130, 2140
Prugniel Ph., Soubiran C., 2001, A&A, 369, 1048
Rudick C. S., Mihos J. C., Frey L. H., McBride C. K., 2009, ApJ, 699, 1518
Sánchez-Blázquez P., Gorgas J., Cardiel N., González J. J., 2006, A&A, 457, 809
Sandoval M. A. et al., 2015, ApJ, 808, L32
Saulder C., van den Bosch R. C. E., Mieske S., 2015, A&A, 578, A134
Schlafly E. F., Finkbeiner D. P., 2011, ApJ, 737, 103
Schweizer F., Seitzer P., 1998, AJ, 116, 2206
Scott N. et al., 2009, MNRAS, 398, 1835
Scott N. et al., 2013, MNRAS, 432, 1894
Seth A. C. et al., 2014, Nature, 513, 398
Sheinis A. I., Bolte M., Epps H. W., Kibrick R. I., Miller J. S., Radovan M. V., Bigelow B. C., Sutin B. M., 2002, PASP, 114, 851
Smith Castelli A. V., Faifer F. R., Richtler T., Bassino L. P., 2008, MNRAS, 391, 685
Strader J., Brodie J. P., Schweizer F., Larsen S. S., Seitzer P., 2003, AJ, 125, 626
Strader J. et al., 2013, ApJ, 775, L6
Taylor M. A., Puzia T. H., Harris G. L., Harris W. E., Kissler-Patig M., Hilker M., 2010, ApJ, 712, 1191
Taylor M. A., Puzia T. H., Gomez M., Woodley K. A., 2015, ApJ, 805, 65
Thomas D., Maraston C., Bender R., 2003, MNRAS, 339, 897
Thomas D., Maraston C., Bender R., Mendes de Oliveira C., 2005, ApJ, 621, 673
Thomas D., Maraston C., Schawinski K., Sarzi M., Silk J., 2010, MNRAS, 404, 1775
Thomas D., Maraston C., Johansson J., 2011, MNRAS, 412, 2183
Toloba E. et al., 2014, ApJS, 215, 17
Trager S. C., Worthey G., Faber S. M., Burstein D., Gonzalez J. J., 1998, ApJS, 116, 1
Usher C. et al., 2012, MNRAS, 426, 1475
van den Bosch R. C. E., Gebhardt K., Gültekin K., van de Ven G., van der Wel A., Walsh J. L., 2012, Nature, 491, 729
van der Marel R. P., de Zeeuw P. T., Rix H.-W., Quinlan G. D., 1997, Nature, 385, 610
van der Wel A. et al., 2014, ApJ, 788, 28
VandenBerg D. A., Brogaard K., Leaman R., Casagrande L., 2013, ApJ, 775, 134
Willman B., Strader J., 2012, AJ, 144, 76
Zhang H.-X. et al., 2015, ApJ, 802, 30

APPENDIX A: STELLAR POPULATION PARAMETERS AND STELLAR MASSES

We derive the stellar population parameters in two different ways. The full set of indices was used by iteratively clipping indices that did not fit the best-fitting model and finding the best model with the

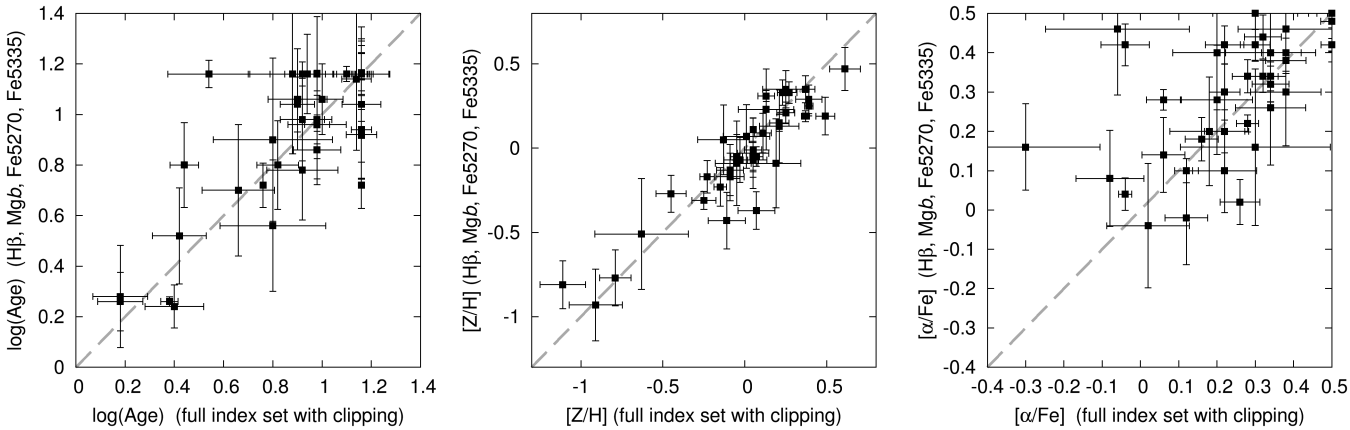

Figure A1. Comparison of the stellar population parameters obtained by fitting the SSP models to different index sets as described in Section 4. The grey lines show the 1:1 relations.

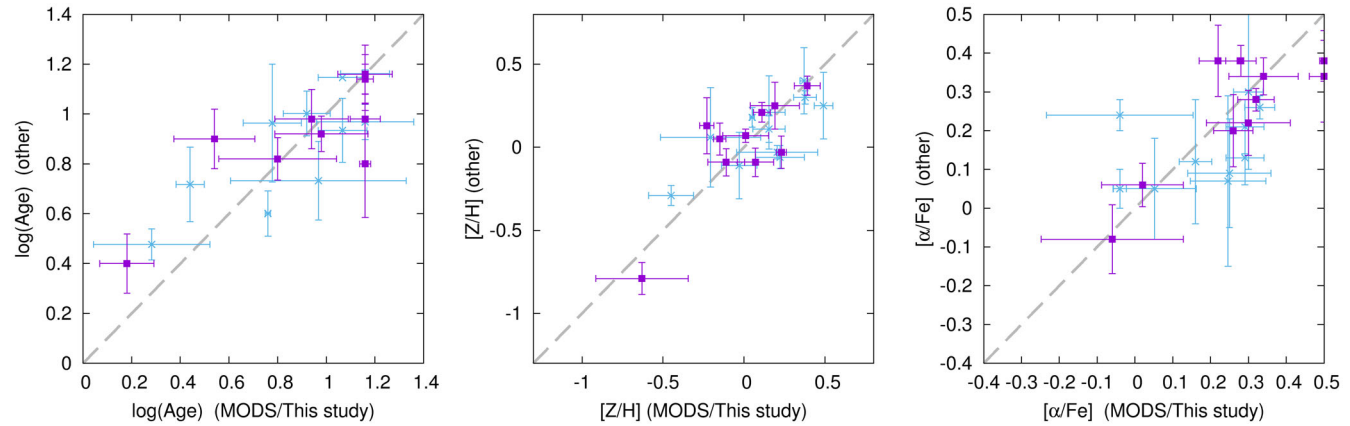

Figure A2. Comparison of the stellar population parameters obtained with different instruments within this study (violet boxes) and to literature (blue crosses). The grey lines show the 1:1 relations.

remaining ones. Alternatively, we used a small index set (Hβ, Mgb, Fe5270, and Fe5335) similar to ATLAS^{3D} (McDermid et al. 2015). In Fig. A1, the comparison of the two is shown. Furthermore, we provide in Fig. A2 a comparison for those objects with two different spectra. For four objects we analysed the SDSS spectra in addition with the same procedures (M85-HCC1, M59cO, cE0, cE2). Also, for several objects (cE0, cE1, cE2, M59-UCD3, M59cO, M60-UCD1, M85-HCC1, NGC 3923-UCD1, NGC 4546-UCD1, NGC 4486B) a comparison of our adopted values to the literature is shown (Sánchez-Blázquez et al. 2006; Chilingarian, Cayatte & Bergond 2008; Huxor et al. 2011b; Huxor et al. 2013; Strader et al. 2013; Liu et al. 2015a; Norris et al. 2015; Sandoval et al. 2015). Given the variety of literature sources with differences in data quality as well as in the stellar population models used for the fitting, the agreement is good. In particular, the metallicities are reliably constrained.

In Fig. A3 our stellar masses are compared to those in the AIMSS I catalogue. Our stellar masses are derived using the spectroscopic SSP stellar population parameters obtained here. This way we can homogenously calculate the masses for all our CSSs and do not need to rely on the heterogenous sets of available photometry. The stellar masses obtained in this way generally show good agreement with those in AIMSS I. Those are based on multiband photometry, but allowing for a composite stellar population with a young and an old component.

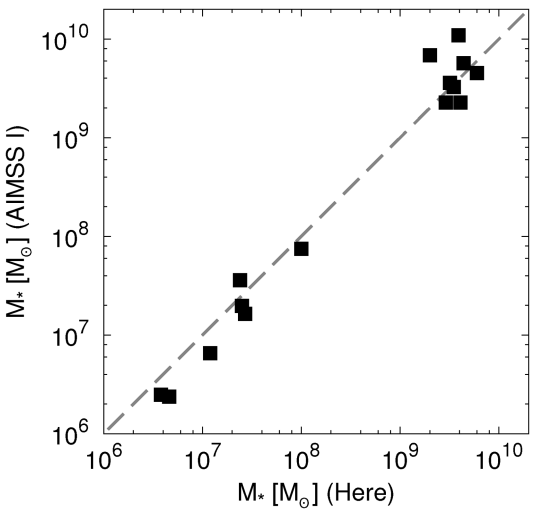

Figure A3. Comparison of the stellar masses obtained from the spectroscopic stellar population parameters here and those in the AIMSS I catalogue, which were determined with broad-band photometry in multiple broad-band filters. The grey line shows the 1:1 relation.

This paper has been typeset from a TEX/LATEX file prepared by the author.